ELSEVIER Nuclear Instruments and Methods in Physics Research A 413 (1998) 397–426

NUCLEAR INSTRUMENTS & METHODS IN PHYSICS RESEARCH Section A

Accelerator-based neutron source for the neutron-capture and fast neutron therapy at hospital

B.F. Bayanov[a], V.P. Belov[a], E.D. Bender[a], M.V. Bokhovko[b], G.I. Dimov[a], V.N. Kononov[b], O.E. Kononov[b], N.K. Kuksanov[a], V.E. Palchikov[a], V.A. Pivovarov[b], R.A. Salimov[a], G.I. Silvestrov[a], A.N. Skrinsky[a], N.A. Soloviov[b], S.Yu. Taskaev[a,*]

[a] *Budker Institute of Nuclear Physics (BINP), Av. Lavrent'ev 11, 630090 Novosibirsk, Russian Federation*
[b] *Institute of Physics and Power Engineering (IPPE), 1 Bondarenko Sq., 249020 Obninsk, Kaluga Region, Russian Federation*

Received 13 February 1998

Abstract

The proton accelerator complex for neutron production in lithium target discussed, which can operate in two modes. The first provides a neutron beam kinematically collimated with good forward direction in 25° and average energy of 30 keV, directly applicable for neutron-capture therapy with high efficiency of proton beam use. The proton energy in this mode is 1.883–1.890 MeV that is near the threshold of the $^{7}Li(p,n)^{7}Be$ reaction. In the second mode, at proton energy of 2.5 MeV, the complex-produced neutron beam with maximum energy board of 790 keV which can be used directly for fast neutron therapy and for neutron-capture therapy after moderation.

The project of such a neutron source is based on the 2.5 MeV original electrostatic accelerator tandem with vacuum insulation developed at BINP which is supplied with a high-voltage rectifier. The rectifier is produced in BINP as a part of ELV-type industrial accelerator. Design features of the tandem determining its high reliability in operation with a high-current (up to 40 mA) H^- ion beam are discussed. They are: the absence of ceramic accelerator columns around the beam passage region, good conditions for pumping out of charge-exchange gaseous target region, strong focusing optics and high acceleration rate minimizing the space charge effects. The possibility of stabilization of protons energy with an accuracy level of 0.1% necessary for operation in the near threshold region is considered. The design description of H^- continuous ion source with a current of 40 mA is also performed. To operate with a 100 kW proton beam it is proposed to use liquid-lithium targets. A thin lithium layer on the surface of a tungsten disk cooled intensively by a liquid metal heat carrier is proposed for use in case of the vertical beam, and a flat liquid lithium jet flowing through the narrow nozzle – for the horizontal beam.

PACS: 29.25.Dz; 87.56. – v; 29.17. + w; 41.75.Cn

Keywords: Neutron therapy; Neutron source; Tandem accelerator; Boron capture

* Corresponding author. Fax: + 7 3832 352163; e-mail: taskaev@inp.nsk.su.

0168-9002/98/$19.00
PII: S0168-9002(98)00425-2

1. Conception of the accelerator-based neutron source for the neutron capture and fast neutron therapy at hospitals

1.1. Introduction

At present, the beam therapy is one of the basic methods for curing malignant tumors. Recently, the ever increasing attention in therapy was drawn to the use of neutron beams. Quite confident evidences of the successful use of neutrons in both the beam and combined therapy of tumors were obtained in the USA, Japan, Germany, Russia, Great Britain and France.

The neutron therapy, i.e. the irradiation of malignant tumor by the neutron flux is presently realized in two versions: a neutron-capture therapy (NCT) and fast neutron therapy (FNT).

NCT, whose idea was proposed in 1936 (in 4 years after the neutron discovery) [1], consists in that the isotope with a large absorption cross-section of thermal neutrons is introduced into the patients body mainly through his/her blood. At present, the most studied and used in clinical practice is the version of the boron neutron capture therapy (BNCT) [2,3]. The boron-containing compounds enriched in the isotope ^{10}B are synthesized. This compound introduced into the patient's blood produce in the tumor cell the ^{10}B isotope with concentration 30 $\mu g\, g^{-1}$ while in the surrounding normal tissue cells to be $\sim 10\ \mu g\, g^{-1}$. In the neutron reaction $^{10}B(n,\alpha)^{7}Li$ the charged particles are produced with the total kinetic energy ~ 2.4 MeV and with a range in a tissue $\sim 10\ \mu m$ i.e. of the order of the size of a man's tumor cell. As a result, the cell comprising ^{10}B is effectively destroyed. Because of higher concentration of ^{10}B-isotope in the tumor cells mainly the cancer cells are destroyed. Thus, the basic idea of BNCT is that a neutron "finds" out the tumor cells and destroys them.

At the same time, some other versions of NCT are presently under consideration which use other isotopes with high neutron absorbtion, for example ^{155,157}Gd [4].

The main requirements of the neutron beam for NCT are the following:

1. Neutron energy should mainly be ranged from 1 eV to a few tens of keV. This region is related to that the cancer tumor is located under the normal tissue at a depth of 30–70 mm. The thermal neutrons (the most intensively absorbed with ^{10}B) weakly penetrate the tissue and produce the major radiation load on the surface layers (primarily on the skin) with no desirable effect on the deep tumor. Epithermal neutrons passing through the normal tissue layers are thermalized resulting in the peak of the thermal neutron flux in the deep tissue and thus providing the maximum of absorbed dose in the irradiated tumor. At the same time, there should be no fast neutrons and the spectrum upper boundary should not exceed a few tens of keV. This is related to the fact that fast neutrons produce the main radiation effect in the tissue the recoiling protons have their maximum on the surface tissues and also have no selective character.

2. The required intensity of a neutron beam is determined by the required absorbed radiation dose in a single treatment and by the desirable exposition duration. The estimates show that at a 10 min exposition, for attaining an absorbed dose of 20 Gy in a tumor with the ^{10}B concentration of 30 $\mu g/g$ the epithermal neutron flux is required to be $(0.5\text{–}1)\times 10^{10}\ cm^{-2}\, s^{-1}$. It is evident that the neutron flux value can be reduced at the same absorbed dose either by the extension of irradiation time or by an increase in ^{10}B concentration in the tumor.

3. It is desirable that the absorbed dose produced by fast neutrons and by accompanying gamma-rays should not exceed 10% of the therapeutical dose, i.e. 2 Gy.

4. The neutron beam should be well collimated, i.e. with a slight divergence and quite distinct boundaries.

The fast neutron therapy uses the fast neutron beams with high penetrability in to the tissue. The main therapeutical effect is achieved due to recoiling protons and heavier recoiling nuclei. The work performed at the Medical Radiological Research Center (MRRC RAMS) in collaboration with Institute of Physics and Power Engineering (IPPE) in Obninsk [5] has shown promising results in the use of a beam of fast neutrons from the BR-10 reactor in curing the old radioresistant tumors. Beginning from 1985, MRRC has conducted the successful

cure of 230 patients with malignant tumors of the head, neck, dairy gland, osteogeneous sarcomas with the neutron beam B-3 from the BR-10 reactor. The main requirements of the fast neutron beam for FNT are the following:

1. The neutron spectrum should be similar to the neutron spectrum of uranium fission. A fraction of neutrons with an energy over 100 keV in the beam spectrum should be 90%.
2. The neutron flux on the collimator output should be $\sim 1 \times 10^9$ cm^{-2} s^{-1}.
3. The dose produced by an accompanying gamma radiation can be 50% of the total dose.

1.2. Neutron sources for NCT and FNT

The nuclear reactor is the most powerful stationary source of neutrons. At a 1 MW heat power in the reactor, $\sim 10^{17}$ neutrons s^{-1} are produced. It is quite natural that the beams of reactor neutrons have been used for the NCT and FNT purposes. At present, in the world there are a few active operating therapeutical beams on the nuclear reactors of various kinds and powers [6]. In addition, detailed projects are published for various therapeutical facilities which to a great extent take into account the medical and radiological requirements of neutron beams [7–9].

Since the neutron spectrum of the reactor core does not satisfy the NCT requirements because of a substantial fraction of fission neutrons, for producing a beam with the required parameters special filters are used. For this purpose, the most frequently used is the composition of the heavy water and aluminum or its oxide in the proportion 1 : 10 with a length of 1 m.

For the attenuation of gamma rays the 10 cm thick Pb or Bi layers are used and thermal neutrons are absorbed by Cd or Li. Such filters can usually be called as scattering filters. The required neutron spectrum is achieved as a result of multiple scattering in quite a lengthy medium moderating neutrons to epithermal energy. On the output of such a filter ~ 1 m thick collimator should be installed to form the beam of required geometric dimensions. Such a structure of a neutron beam formation for NCT leads to that for providing the necessary beam intensity with the required spectral characteristics one has to get quite a high neutron flux in the reactor core and as a consequence, its average power density in core and substantial power of reactor. For example, the MTR reactor designed for medical research has a power of 10 MW. Some other reactors developed as sources of neutrons for NCT have a power ranging from 5 to 20 MW.

Another approach for the formation of a neutron spectrum required for NCT [9] is the use of a special filter made of material with a large neutron cross-section at an energy of neutrons above ~ 10 keV and a small neutron cross-section in the range of epithermal neutrons. A ^{64}Ni isotope can be served as an example of such a filter. This filter is a transmission-operated filter removing from a beam the neutrons with energies over 10 keV and enabling the passage of useful epithermal neutrons for NCT. The use of the transmission filter enables one to achieve the required beam parameters as, for example, in the use of the fluid fuel reactor of 200 kW in power [9].

The main characteristics of the reactor neutron beams for NCT are given in Table 1.

In Obninsk the studies of the fast neutron therapy have been conducted within the frame of collaboration between two research centers for over 10 years namely the IPPE having the fast neutron reactor BR-10 at a power of 6 MW with the sodium coolant carrier and the MRRC RAMS where the methods of beam therapy are developed and the complex cure of cancer tumors is performed. The FNT is realized on the horizontal neutron beam of the B-3 reactor with maximum sizes of 10×10 cm^2. The neutron spectrum is broad enough with mean energy of 0.8 MeV. The density of the fast neutron flux is 3×10^8 cm^{-2} s^{-1}. The typical treatment time is 10–20 min. The fluid fuel reactor whose project was developed at IPPE enables one to get the fast neutron beam for FNT with a flux density of up to 2.5×10^{10} cm^{-2} s^{-1}.

In conclusion of the brief description of neutron beam characteristics for FNT and NCT based on nuclear reactors let us note some of their advantages and disadvantages:

1. Although the existing beams for NCT do not provide the necessary flux density and require large expositions (≥ 60 min), the neutron beams of

Table 1

Reactor	Power (MW)	Filter	F_{epith} ($cm^{-2}\,s^{-1}$)	Treatment time (min)
MTR (INEL)	10	$Al/D_2O/Li$	1.7×10^{10}	10
MIT R-II (MIT)	5	$Al/D_2O/Li$	4×10^{9}	40
BMRR (BNL)	3	$Al/D_2O/Li$	1.8×10^{9}	90
Solution (IPPE)	0.2	$^{64}Ni/Al/S$	2.8×10^{9}	60

designed special medical reactors satisfy the basic requirements for NCT and FNT in their spectral characteristics and treatment times ($\geq$ 10 min).

2. The nuclear reactor in its stationary regime of operation has a constant power level and the beam composition thereby providing standard expositions.

The following factors can be considered as serious disadvantages of reactor therapeutical facilities:

1. A powerful reactor is a very complex and expensive facility whose maintenance demands quite strong requirements for nuclear safety.
2. With quite a rare exception, the cancer therapy centers and clinics are usually remote from the physics centers having nuclear reactors.

These circumstances in recent years, have led to intensive discussions on the problems of developing a neutron source for NCT based on the compact and inexpensive accelerator which can be used for every cancer clinic.

At present, various versions of neutron sources for NCT using cheap accelerators of direct action are conceptually developed [10,11]. For obtaining neutrons the nuclear reactions on light nuclei such as $T(p,n)^3He$, $^7Li(p,n)^7Be$, $^9Be(p,n)^9B$ and other are supposed to be used. For obtaining neutrons in these reactions there is a need to have protons with energies up to 2–2.5 MeV.

The problems hindering the development of an intense accelerator-based neutron source for NCT are regularly discussed in the biannual International Symposia on the neutron capture therapy of cancer and in the International Conferences on the applications of accelerators in science and technology. In 1994, in Jackson (USA), the 1st International Workshop "Accelerator-Based Neutron Sources for BNCT" was held. In those meetings, several projects of high-current compact accelerators applicable to the development of neutron sources for NCT were presented.

1.3. Parameters of neutron source based on the reaction $^7Li(p,n)^7Be$

The reaction $^7Li(p,n)^7Be$ is widely used for obtaining monoenergetic neutrons in nuclear physics experiments and it is quite well studied [12]. This reaction is the threshold reaction. The reaction energy is $Q = -1.644$ MeV and the threshold value of proton energy is $E = 1.881$ MeV.

1.3.1. Near-threshold region

There is a broad resonance with $J = 2^-$ near the threshold. Because of this resonance, the reaction cross-section increases sharply over the threshold value and it has foot-step form. The neutrons escaping the reaction near the threshold have an orbital momentum $l = 0$ and, consequently, an isotopic angular distribution in the center-mass system (CMS). These two important circumstances enable the description of the spatial-energy distribution of escaping neutrons in the laboratory system (LS) with the help of analytical expressions [13–15]. Using a simple approximation of the homogeneous stopping of protons in lithium due to ionization losses these analytical expressions have the form

$$Y_{\pm} = 3\times10^3\sqrt{E_p - 1881}\left(1 + 6\sqrt{\frac{E_p - 1881}{E_p}}\right)^{-2} \times \frac{\alpha(Z \pm \cos\psi)}{Z\cos\psi \pm (49 - \sin^2\psi)},$$

where $Y_{\pm} = d^2n/dE_n\,d\omega$ [neutron/(eV sr μC)] – is a doubly differential yield (DDY) of neutrons per the unit of their energies per the unit of solid angle and per 1 μC of protons; ψ is an escaping angle of

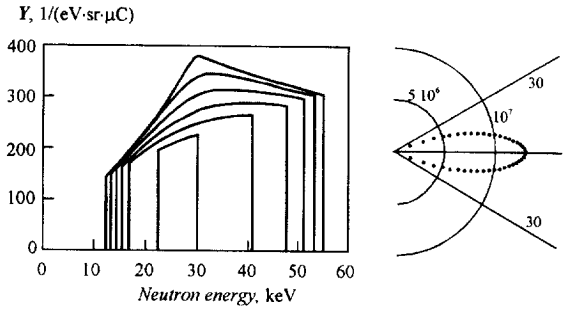

Fig. 1. The doubly differential yield of neutrons from a thick metallic-lithium target for various laboratory escape angles (angle step is 5°) and angular distribution of neutrons in polar coordinates at an initial proton energy of 1886 keV.

neutrons in LS with respect to the direction of the proton beam; E_p is an energy of protons [keV], Z and α are dimensionless parameters determined by the following relations:

$$Z^2 = \alpha^{-2} - \sin^2\psi,$$

$$\alpha^2 = M_p M_n E_p [M_{Be} M_{Li}(E_p - 1881)]^{-1},$$

comprising masses of interacting particles. An energy of neutron in LS is determined by the following relation:

$$E_{n\pm} = \frac{M_n M_p}{(M_{Be} + M_n)^2} E_p (Z \pm \cos\psi)^2.$$

Signs " + " and " − " evidence the double character of energy value for neutrons and DDY at $\alpha > 1$ which correspond to neutrons escaping CMS into the front and back hemispheres, respectively.

The relations given enable one within the frame of declared approximations to calculate an energy distribution and an absolute yield of neutrons from a thick metal lithium target. The relations are valid up to the proton energy level of ~ 1920 keV which corresponds to $\alpha = 1$.

Fig. 1 shows the doubly differentiated yield of neutrons from a thick metal lithium target and an angular distribution of escaping neutrons in LS in the polar coordinates at an initial proton energy of 1886 keV.

Note the important NCT features of the neutron source based on the use of the reaction ^{7}Li(p,n)^{7}Be in the near-threshold region.

1. The source has a well distinct direction ahead related to the specificity of kinematics of the threshold nuclear reactions (the so-called "kinematics collimation").
2. The spectrum of neutrons lies in the energy region ~ 15–50 keV acceptable for NCT and it has the distinct upper boundary determined by physics conditions with no "tail" of fast neutrons.

These circumstances enable one to consider the possibility of using such a source for the irradiation in the open geometry at a short distance between the source and subject without the use of an external collimator.

Table 2 shows the calculated value of the total yield of neutrons from the ^{7}Li(p,n)^{7}Be reaction and limit escaping angle in the near-threshold region.

Since for the use in NCT quite broad neutron beams are required which are determined by the

Table 2

Proton energy (keV)	Total yield neutrons at 10 mA (s^{-1})	Limit angle of escape (grad)	Limit energy of neutrons (keV)
1883	8.47×10^9	13.2	44.8
1884	1.46×10^{10}	16.1	48.7
1885	2.15×10^{10}	18.6	52
1886	2.91×10^{10}	21	55.1
1891	7.11×10^{10}	30.9	67.9
1896	1.18×10^{11}	38.2	78.6
1901	1.67×10^{11}	45.4	88.3
1911	2.71×10^{11}	60.5	105.9
1920	3.66×10^{11}	81.7	120.6

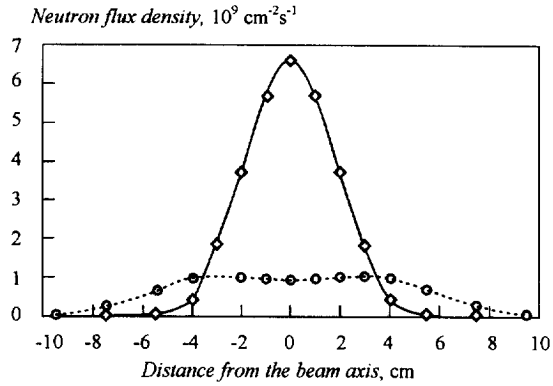

Fig. 2. The radial distributions of neutron flux in planes remote from the target at distances 3 cm (◇) and 10 cm (○) for incident proton energy of 1896 keV and beam current of 10 mA.

tumor sizes, it is reasonable to use the targets of ~ 5 cm in diameter. In this case, the problem of reducing a power density in the target is simultaneously solved. For obtaining a flux density and neutron spectrum produced by such a source under conditions of finite geometry the calculations were performed [16] by the Monte-Carlo method with the use of the MCNP-4A code.

Fig. 2 shows the radial distributions of the neutron flux in planes remote from the target at the distances 3 and 10 cm for incident proton energy of 1896 keV and a been current of 10 mA. In the first case, the maximum value of neutron flux is 6.5×10^9 cm^{-2} s^{-1} and the diameter at 0.1 of the maximum flux is ~ 7 cm. In the second case, the neutron flux is 10^9 cm^{-2} s^{-1} and the characteristic beam diameter of 20 cm is achieved.

The calculations of spatial distribution of an absorbed dose performed with MCNP-4A code have shown that such a neutron source at a distance between the object and target of 3 cm can produce at a depth of 5–7 cm the required therapeutical dose of 20 Gy after an exposition of 10 min. The more detailed calculations enable the choice of optimum operation conditions of the source. However, the bench computation seems promising for NCT use of the naturally collimated beam of neutrons from the reaction ^{7}Li(p,n)^{7}Be in the near-threshold region under the conditions of open geometry. The accelerator main parameters required for the development of such a source are the following:

- proton energy $E_p = 2$ MeV,
- energy stability 0.1%,
- proton beam current 10 mA,
- beam current density 0.5 mA cm^{-2}.

1.4. ^{7}Li(p,n)^{7}Be reaction as a source of epithermal and fast neutrons

With an increase in proton energy the neutron escape angle is turned by 4 π rad at $E_p \approx 1920$ keV and the total neutron yield increases up to 1×10^{13} s^{-1} at an energy of protons 2.5 MeV and a beam current of 10 mA. At such intensity it turns out possible to produce the source of appropriate epithermal neutrons for NCT by the formation of the required spatial-energy distribution of neutrons with the help of the compact moderator–collimator unit. The design and optimization of such a unit requires the initial data on the spatial-energy distribution of primary neutrons from the thick lithium target. The data can be found out by using the following relations:

$$Y = \frac{6.19(\mathrm{d}\sigma/\mathrm{d}\omega)}{(\mathrm{d}E_p/\mathrm{d}x)(\mathrm{d}E_n/\mathrm{d}E_p)},$$

where Y is the DDY [neutron/(eV sr μC)], $\mathrm{d}\sigma/\mathrm{d}\omega$ the differential cross-section of the reaction ^{7}Li(p,n)^{7}Be [mb/sr],

$$\frac{\mathrm{d}E_n}{\mathrm{d}E_p} = \frac{(\cos\psi + Z)}{(M_{Be} + M_n)^2}\left[M_p M_n(\cos\psi + Z) + \frac{M_{Be}M_{Li}1881}{ZE_p}\right],$$

$$\frac{\mathrm{d}E_p}{\mathrm{d}x} = \frac{718}{E_p}\left[\ln\frac{E_p}{3000} + 4.96\right][10^{-15}\ \mathrm{eV\ cm^2}],$$

$$E_n = \frac{M_p M_n}{(M_{Be} + M_n)^2}E_p(\cos\psi + Z)^2,$$

and E_p, E_n are proton and neutron energies [keV].

The values of the differential cross-section of ^{7}Li(p,n)^{7}Be were quite exactly measured in the broad region of proton energies and then evaluated and summed in tables by Liskien and Paulson [17].

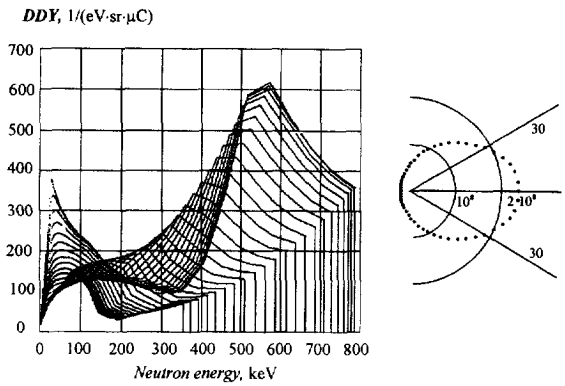

Fig. 3. The doubly differential yield of neutrons from thick a metallic-lithium target for various laboratory escape angles (angle step is 5°) and angular distribution of neutrons in polar coordinates at an initial proton energy of 2.5 MeV.

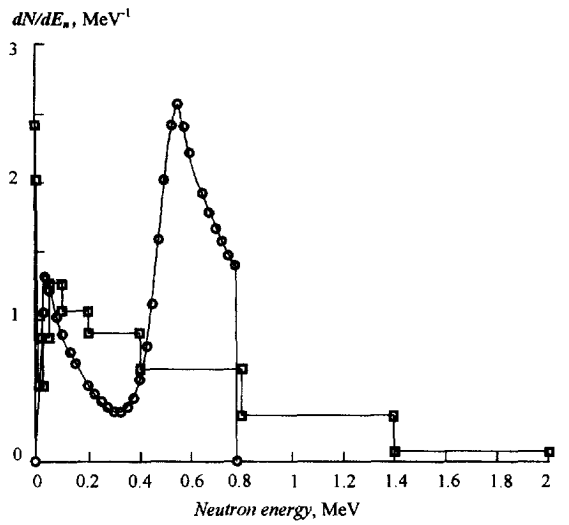

Fig. 4. Energy neutrons spectrum for ^{7}Li(p,n)^{7}Be reaction at 0° laboratory angle and initial proton energy 2.5 MeV and neutrons energy distribution for BR-10 reactor's medical neutron beam B-3.

These relations enable the calculation of an absolute yield and the spatially energy distribution of neutrons from this reaction within the proton energy range over 1920 keV.

Fig. 3 shows the calculation results for DDY neutrons from the thick lithium target at a proton energy of 2.5 MeV. The calculations of the spatial-energy distribution of the absorbed dose performed for the optimum moderator–collimator unit with an output window made of beryllium oxide of 20 cm thickness have shown that such a version of the source of epithermal neutrons for NCT provides the absorbed dose 20 Gy at a depth of 5–7 cm for an exposition of 100 min.

The reaction ^{7}Li(p,n)^{7}Be at an energy of protons of 2.5 MeV is also a convenient source for FNT. In this case, one has to use the neutrons moving ahead with no attenuation. Such a source can be arranged by putting the target into the compact safeguard unit made of LiH having the collimating-output window.

Fig. 4 shows the comparison of neutron spectra normalized to 1 from such a source and B-3 neutron beam of BR-10 reactor widely used for FNT. It is seen that neutron spectra are quite close and the radiobiological efficiency of fast neutrons from ^{7}Li(p,n)^{7}Be reaction should be close to that of the B-3 beam reactor neutrons. The fast neutron flux from the reaction ^{7}Li(p,n)^{7}Be at the proton energy of 2.5 MeV and beam current of 1 mA at a distance of 20 cm from the target is 4×10^{8} cm^{-2} s^{-1}, i.e. it has the same value as that for the B-3 beam.

The requirements of the accelerator for producing the source of epithermal neutrons and the source of fast neutrons are the following:

- proton energy 2.5 MeV,
- energy stability 20%,
- beam current of the source of epithermal neutrons $\geq$ 10 mA,
- beam current of the source of fast neutrons 1 mA.

1.5. Nuclear-physics characteristics of metal-lithium target for the production of neutrons

The proton's range with the energy of 2.5 MeV in metallic lithium is equal to 300 μm, and at the threshold of the ^{7}Li(p,n)^{7}Be reaction they are stopped in a 100 μm thick lithium layer. This data should be taken into account in the design of the target. The target can be made either by surfacing or vacuum evaporation onto the substrate. Evaporation can be done directly in the accelerator vacuum volume [18] thereby avoiding the oxide and

nitrite layers on the working surface which appear inevitably when lithium comes in contact with air.

The product of the nuclear reaction $^{7}Li(p,n)^{7}Be$ is the radioactive nuclide ^{7}Be having a half-life time of 53.5 days. A 90% decay of ^{7}Be proceeds by the radiationless K-capture and 10% by the positron decay accompanied by the emission of gamma-rays with an energy of 0.477 MeV. Thus, the irradiated target is a source of gamma radiation with energies 0.477 and 0.511 MeV. The activity after an hour exposure by 10 mA proton current is 2.33×10^{9} Bk, i.e. ~ 60 mCi. Such an activity of the irradiated target is not a serious radiation danger either for target maintenance or for the patient. However, this activity should be taken into account in the work with the target since the contact with air produces the lithium volatile compositions.

In addition to neutron reactions, at the bombardment of ^{7}Li by protons the nuclear reactions occur emitting gamma rays: $^{7}Li(p,p',\gamma)^{7}Li$ and $^{7}Li(p,\gamma)^{8}Be$. In the first reaction, gamma rays of energies 0.477 MeV are emitted, in the second reaction, the hard gamma rays with energies 14.7 and 17.6 MeV are emitted. The output of hard gamma rays is negligible in comparison to the soft gamma-rays. The output of gamma rays with energy 0.477 MeV from a thick lithium target with proton beam current of 10 mA and energy 2 MeV is $\sim 2.5 \times 10^{11}\ s^{-1}$. When irradiating in open geometry for a 3 cm distance to object, the absorbed dose caused by gamma rays from the $^{7}Li(p,p')^{7}Li$ reaction with energy 0.477 MeV and exposure time 10 min will be 4 Gr at 10 mA proton current, i.e. not more than 5% of necessary therapeutical dose is considered admissible. While using the source of epithermal neutrons for NCT, produced by moderating neutrons from the $^{7}Li(p,p')^{7}Li$ reaction with protons of energy 2.5 MeV there is an additional possibility of attenuation of gamma rays by means of lead or bismuth shielding around the target. Such shielding with a thickness of 1.5 cm decreases the absorbed dose of gamma rays by 15 times and the space-energy distribution of neutrons is not affected by this protection. If necessary lead or bismuth shielding can be used for the source of fast neutrons for FNT, also.

It should be noted that target design must exclude the hitting of a beam or scattered protons in materials with low nuclear excitation levels. For this aim the inner surface of an ion-guide should be covered by materials with high (p,p') reaction threshold – graphite, for example.

2. Main elements and arrangement of the accelerator complex

Selecting the variant of an accelerator for the neutron source, it is desirable to provide the possibility of operation in two regimes, considered before, both in the near-threshold region allowing to use the source for irradiating in open geometry without an external collimator and for the production of epithermal and fast neutrons at proton energies of 2.5 MeV with moderators. But in spite of the attractiveness and elegance of the operation in the near-threshold region such a method of neutron production demands a high monochromaticity and stability of the energy of the proton beam ($dE/E = 0.1\%$). This demand makes the use of the widely discussed variant of the high-frequency accelerator of RFQ type impossible and may be satisfied only by the electrostatic one.

In this project we offer to create the neutron source based on the construction of a vacuum insulation tandem accelerator developed at BINP using the sectionalized rectifier from the electron accelerator of ELV type as a powerful source of high voltage. This kind of accelerators (ELV) was developed at BINP and now is in serial production. Advantages of tandem in comparison to the accelerator on full energy from the point of providing maximum reliability in works with high-current continuous beam are obvious: the ion source is placed under ground potential and the operating voltage is only half of the full proton energy of 1.25 MeV. The design of vacuum insulation tandem discussed in detail in Section 3 provides the reliability significantly exceeding the reliability of tandem based on accelerating columns with the ceramic insulators, also. The reliability of the high-voltage ELV rectifier was confirmed by many years of operation of such accelerators in the industry. More than 70 of ELV-type accelerators were delivered by BINP for operation in Russia's industry

and abroad. The use of such a rectifier as a high-voltage source for tandem supplying is attractive also due to its high efficiency (more than 90%) and for power of proton beam exceeding 20 kW which is enough to make it an important factor for work in hospitals. Design of such a transformer and the possibility of obtaining 0.1% voltage stability are discussed in detail in Section 4.

A possible variant of the accelerator complex arrangement is shown in Fig. 5. The whole installation is placed in a two-floor building in four separate rooms. The high-voltage source (HVS) and main powerful power supply sources are mounted in one of the rooms (I) of the first floor. The accelerator-tandem is mounted through the hole in ceiling above the HVS, so that its main part – vacuum tank with inputting insulator, potential electrodes and charge-exchange target is situated or the second floor (II). The axes of accelerated and injected beams have about 1 m distance above the floor of the second floor. From one side of the accelerator the source of H^- with the differential vacuum pumping system and the optical system of beam transport for injection in the accelerator are placed. The beam after charge-exchange process accelerated up to 2.5 MeV (doubled energy) comes from the other side of tandem and then the parallel shift system displaces the beam to the transport channel. This system separates the high-intensity proton beam and low-current beam of neutrals which can be used both to control the efficiency of the charge-exchange process and for precise measurements

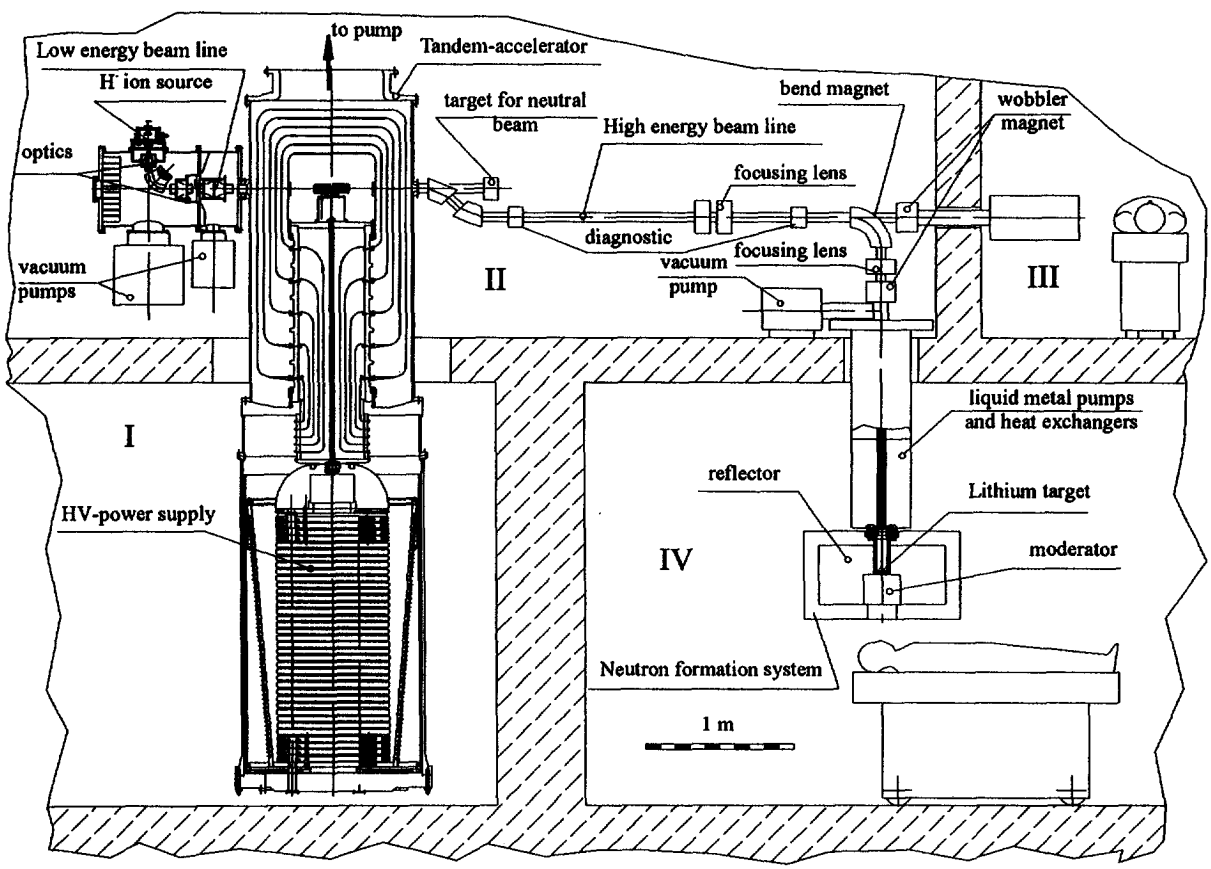

Fig. 5. Possible variant of accelerator complex.

(after additional stripping) of beam energy by means of special bending magnets.

The proton beam is directed by the transport channel (high-energy beam line at Fig. 5) in two medical rooms. The horizontal beam enters the medical room III for works with vertical jet liquid-lithium-neutron-producing target. The heat removal of power released by the proton beam is realized by pumping of liquid lithium through the heat exchanger. The transport channel has 90° bending magnet which directs the beam through a hole in the floor to another neutron-producing target situated in the irradiation room IV at the first floor. This target is a tungsten disk cooling intensively by water or liquid metal coolant and covered by a thin layer of lithium on which the proton beam is made to fall. Such a target can operate both with solid and liquid lithium, therefore, it can be used only with the vertically directed proton beam.

Lithium neutron-producing targets are described in detail in Section 6. They are the most responsible and stressed elements of the whole complex, because all the power of the proton beam (more than 20 kW) is dissipated in the thin lithium target.

To obtain an uniform distribution of the beam on the surface approximately 5 cm in diameter a method of recirculating scanning by means of a wobbler magnet is used. This magnet is a rotating dipole of cobalt–samarium magnets. Possibility of using two variants of the target is foreseen – the open target to work in the region near the threshold and the target with the moderator and reflector. The moderator and reflector are used for space-energy forming of epithermal neutron beam and consist of a combination of cylindrical shape blocks filled with D_2O, BeO, MgO, Al_2O_3 (Fig. 17). The composition and size of the moderator–reflector were optimized by neutron-physical calculations using the MCNP program complex. Such work was carried out in several scientific centres (MIT, Ohio Univ., Univ. of Birmingham [10,11]). The experimental study of space distribution of neutrons of this source in phantom had also a place. It is planned to continue works under optimization of moderator-reflector to specify its design and composition.

3. High-current accelerator-tandem with vacuum insulation

In the conventional scheme of the tandem, two accelerating columns based on ceramic tubes are connected by the high-voltage parts with the charge-exchange target in between. The prospect of the high-current (a few tens milliamperes) accelerator design according to this scheme is limited by its two basic disadvantages – the necessity of pumping the gas charge-exchange target through accelerating columns and an inevitable current emission of secondary electrons and ions from the high-current beam passage region to the inner surface of the ceramic insulators. Both these factors reduce substantially the high-voltage strength of the accelerating columns and require a substantial increase in their transverse and longitudinal dimensions.

In the tandem developed by us there are no ceramic accelerating columns. In this scheme, to the cylindrical potential electrode with charge-exchange target, placed a vacuum tank, high voltage is applied through the ceramic inputting insulator which, in principle, can be arbitrarily remote from the accelerated beam passage region.

The high-voltage electrode is surrounded by a system of different potential shields providing the homogeneous distribution of the potential and preventing the full voltage effects. In the walls of vacuum tank, potential electrode and in the shields are coaxial round holes for the beam passage which is accelerated and focused during its passage. Since the thin-wall shields placed along the equipotential surfaces of the electrostatic field hardly contribute to focusing, the beam focusing in this system is only provided by two axisymmetric lenses – by the lens strongly focusing the low-energy beam in the input hole of the grounded wall of vacuum tank and by the lens defocusing the already accelerated beam placed in the hole of the potential electrode. The specific feature of such a focusing system with high rate of acceleration is considered below in more detail (Section 3.1).

The efficient pumping of the inner cavity of the potential electrode with the gas target placed inside is produced through its upper cover and through removable covers of cylindrical shields. These

covers made of vacuum transparent as they have a large number of sector holes displaced with respect to each other along the azimuth to prevent the direct passage and acceleration of the particles.

The charge-exchange target is a pipe with an inner hole of 4 mm in diameter and 260 mm in length. At the center of the pipe, the gas (nitrogen, air) leaks at a rate providing the efficient density of the target 3×10^{16} mol cm^{-2} required for the charge-exchange. As shown in Section 3.2, in the geometry under consideration at a given rate of gas leak, the pressure distribution in the whole volume, required for the high-voltage strength of a gap, is provided at a pumping rate ~ 2500 l s^{-1}.

The most important component of an accelerator is the high-voltage inputting insulator through which the potential is transferred into the vacuum cavity from the tank filled with SF_6 gas with the transformer of the ELV-type industrial accelerator being the powerful source of high voltage. The high-voltage input is a thick walled ceramic tube 45 cm in diameter and 120 cm in length with five metal rings fixed on its outer surface for the fixation of cylindrical shields surrounding the central potential electrode. The potential electrode is placed on the insulator end of the metal flange which is vacuum tightened to the end of the ceramic tube by the tightening rod passing along its axis connected to the high-voltage source. On the opposite side of the input (placed in SF_6) the rod is tightened to the second end flange supported by the nonvacuum part of the insulator formed of six rings of organic glass separated by metallic rings for the potential distribution. The voltage is applied to these rings from the resistive–capacitive divider providing the homogeneous distribution of the potential along the insulator length. Inside the insulator around the tightening rod five thin walled pipes of various lengths are concentrically located to connect the respective rings of different potentials on the vacuum ceramic part of the insulator and its lower part placed in SF_6 gas.

The radial gaps between the cylindrical shields in the vacuum part of the accelerator are selected to be of 4 cm so that at the voltage of 1.25 MV on the potential electrode the potential difference between shields is ~ 200 kV and the maximum electric field intensity does not exceed 60 kV cm^{-1}. The field intensity on the surface of the ceramic insulator, divided along its length by six metal rings into six sections 20 cm each, is less than 10 kV cm^{-1}. In the insulator's inner part filled with SF_6 gas, the radial separation of the potential around the central tightening rod is provided by the thin wall cylindrical tubes and their geometry is selected in such a way that the maximum field intensity in SF_6 gas at a pressure of 3 atm does not exceed 70 kV cm^{-1}. Such intensities of electric fields seem to be quite moderate so one can expect a very reliable operation of the high-voltage input from the viewpoint of the electric strength. As an insulator it is planned to use a widely used ceramic insulator of the type P1240/450 UHL1 in electrotechnical industry which needs a slight modification for fitting and connection of the inner and outer metal rings fixing the cylindrical shields of potential separation.

The prototype of such a tandem with vacuum insulation at an energy of 1 MeV is presently used successfully as an injector of the compact proton synchrotron (Fig. 6).

The high-voltage source is a cascade multiplier at a voltage of 0.5 MV. The potential electrode is surrounded by two shields with 3 cm gaps and voltage of 170 kV between each other. The tandem is operated with a pulse source of negative ions providing the current up to 8 mA at a pulse duration of 10 μs. At present, a pulse gas (air) target is used as the charge-exchange target. This is a 16 cm long pipe with the inner diameter of 0.8 cm with a pulse (1 ms) gas pumping in the center of the tube. The stationary gas target being tested on the special vacuum stand is planned to be installed on this tandem.

3.1. Tandem optics

The specific feature of the tandem optics is determined by the design of its potential electrodes. The edges of round holes in the walls of the input are grounded, and potential electrodes have roundings to eliminate the higher intensities of the electric field. At the same time, for the electrodes with distributed potential, the repeating equipotential

Fig. 6. Photo of the tandem prototype. (1) tandem, (2) synchrotron.

field surfaces are desirably to be made of minimum thickness for eliminating the transverse components of the field in the holes generating excessive intensities and beam focusing. From the design viewpoint their thickness was chosen to be 1 mm. This enables the minimum gap between the potential electrode and the grounded tank wall determined only by the admissible field intensity between the electrode metal surfaces and also enables one to provide the maximum rate of particle acceleration. In the geometry selected the total energy growth of 1.25 MeV is achieved at a length of 24 cm. The energy of H^- ions injected into the tandem is 25 keV.

The second specific feature of the tandem is that there is only one strongly focusing lens in the tandem input hole where the particle energy is still low. The second (defocusing) lens in the potential electrode input hole is weak since here the beam has already high energy. The high rate of acceleration reduces the longitudinal size to its minimum in the area of the input lens where the space charge has a substantial effect. The focal distance of the input lens is determined by its hole diameter. Fig. 7 shows dependencies of the focal distance on holes diameter.

Focal distance of the lens increases if the hole in the thick wall is made not of round but of cone shape. In our geometry, the diameter of all the holes are selected to be of 50 mm, the input hole on the output shifts to the cone with a resultant of 45° and a base of 110 mm. As a result, the lens focus is placed at a distance of 80 mm from the tank's inner surface (the tank inner diameter is 530 mm). The crossover for the converging beam transported from the outer source of negative ions should be located here. For each current value the optimal convergence angles should conform with the beam divergence from the crossover under the action of space charge. Fig. 8a shows the characteristic particle trajectories in the tandem. The upper curve is the laminar flow envelope of 50 mA. Fig. 8b shows the envelope of the nonlaminar beam and the longitudinal electric field diagram.

The tandem acceptance is determined by the geometry of the charge-exchange target. For the charge-exchange tube of 180 mm in length and 4 mm in diameter the tandem acceptance in front of

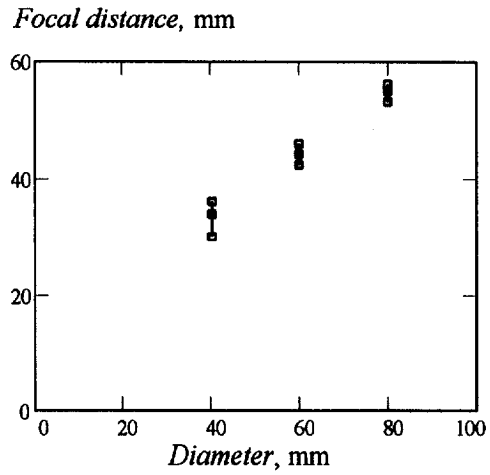

Fig. 7. Dependencies of the focal distance (a distance to the axis intersection point from the tank inner surface) on holes diameter. The particles direct backward from the second shield in parallel to the axis (point from above - radius 5, 10 and 15 mm).

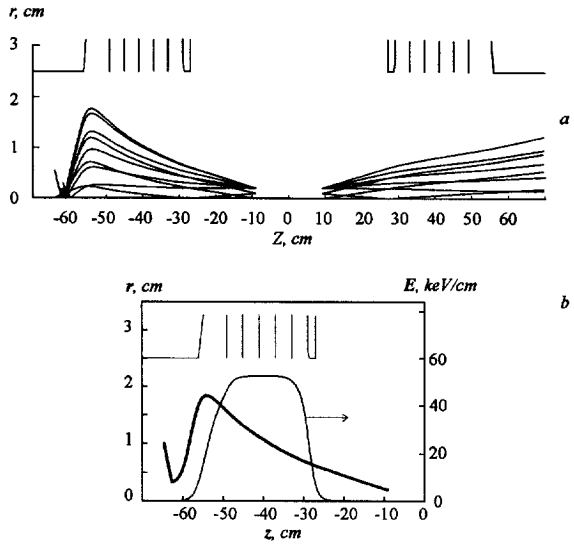

Fig. 8. (a) The characteristic particle trajectories in the tandem without regard for space charge and the envelope of 50 mA laminar flow (the upper curve is in the range of negative z); (b) The envelope of non-laminar 50 mA beam. A diagram of longitudinal electric field is also shown. Note that longitudinal and transverse scales differ. The electrode surfaces are shown in the area $r \geq 2.5$ cm.

the input lens without regard for space charge of a beam is given in Fig. 9a. The acceptance shape distortion is the result of spherical aberration of lenses. The emittance diagram of 50 mA beam in front of the input lens is given in Fig. 9b. The beam will have a homogeneous distribution of current density in the charge exchange target.

Comparison of tandem acceptance without regard for space charge (Fig. 9a) and the one with consideration for space charge of 50 mA beam (Fig. 9b) shows the tandem optics to have low sensitivity to current.

At the finite thickness of a shield, its hole is operated as a weak focusing lens. The focusing effect of shields is numerically calculated for the thickness of 1 mm, the hole diameter of 50 mm and the gap between shields of 40 mm. For finding out the effect of an individual shield it was assumed that the previous and next shields have no holes. Particles from the previous shield directed parallel to the axis with different transverse coordinates upon passage the hole acquires a small diverging angle which is practical linearly dependent on the coordinate, i.e. the hole in the first shield acts as a lens with a large focal distance of 30 m. All the next lenses have lower affect on the beam because of the energy increase.

The shields have the shape of cylinders that leads to the appearance in one plane of radial electric field focusing the beam. For the first shield, the focal distance of the generating lens is 4 m that influences weakly on the beam focusing during the passage of tandem. This focal distance can be increased by local decreasing of shield curvity.

3.2. Charge-exchange target

The effective pumping of the inner cavity of the potential electrode with the gas target located inside is performed through its upper cap and through the caps of cylindrical shields. The holes in the caps are blocked by the symmetrically located sectors. The sectors of the neighboring caps are shifted along the azimuth to prevent the direct passage of accelerated particles since this might cause the multiplication of accelerated particles due to secondary emission.

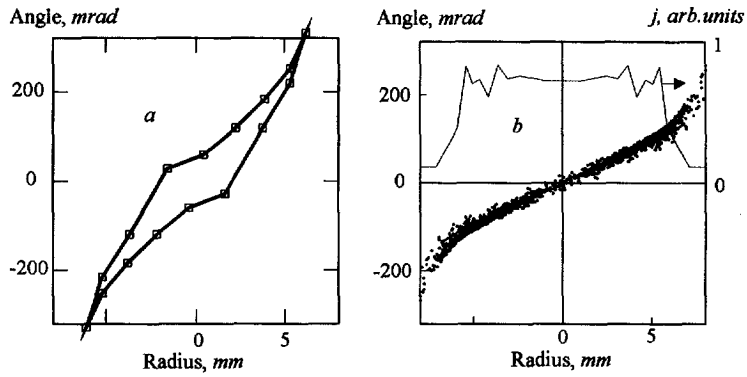

Fig. 9. (a) Charge-exchange tube acceptance without regard for space charge in front of the input lens (on distance of 60 mm from the tank inner surface); (b) 50 mA beam emittance with homogeneous distribution of current density in the charge exchange tube in front of the input lens (on distance of 60 mm from the tank inner surface).

3.2.1. Description of charge-exchange target

The charge-exchange target is a tube having an inner diameter of 4 mm and of length 260 mm. In the center of the tube, the gas is filled to provide the target density required for the charge exchange. The process of charge exchange of negative ions is related to the process of the charge exchange of protons into neutral particles, protons into negative ions, neutral particles into protons, neutral particles into negative ions, negative ions into neutral particles, and negative ions into protons with cross-sections σ_{10}, σ_{1-1}, σ_{01}, σ_{0-1}, σ_{-10}, σ_{-11}, respectively. At a particle energy of 1 MeV the following inequalities take place $\sigma_{1-1} \ll \sigma_{10} \ll \sigma_{0-1} \ll \sigma_{-11} < \sigma_{01} < \sigma_{-10}$. Neglecting the processes of the electron capture we get the dependence on the proton concentration θ_+ on the target thickness δ.

$$\theta_+ = 1 - \frac{\sigma_{-10} - (\sigma_{01} - \sigma_{-11})e^{-(\sigma_{-10}+\sigma_{-11}-\sigma_{01})\delta}}{\sigma_{-10} + \sigma_{-11} - \sigma_{01}} e^{-\sigma_{01}\delta}.$$

Using the experimental data on the charge-exchange cross-sections (see Table 3) and reasoning from the necessity to provide 99% yield of protons one can find the target thickness δ.

We can find the ionization losses of energy E_{los} using the Bete formula [19]

$$E_{los} = \eta\delta,$$

$$\eta = 8\pi a_0^2 Z I_i \left(\frac{\alpha}{\beta}\right)^2 \left[\ln\left(\frac{4I_i}{ZB}\gamma^2\left(\frac{\beta}{\alpha}\right)^2\right) - \beta^2\right].$$

The mean square of energy loss dispersion on the path of 1 atom cm^{-2} is

$$\Delta W_{disp} = 16\pi a_0^2 Z I_i^2 \left[1 + \frac{ZB}{2I_i}\left(\frac{\alpha}{\beta}\right)^2 \ln\left(\frac{4I_i}{ZB}\left(\frac{\beta}{\alpha}\right)^2\right)\right].$$

The mean dispersion of energy losses on the whole path is: $\Delta E_{los} = \sqrt{\Delta W_{disp}\delta}$.

The results of the calculation are shown in Table 3.

3.2.2. Calculation of gas consumption

The tube conductivity is calculated for the molecular regime by the formula [20]

$$U = \frac{\pi}{12} v_a \frac{d^3}{L},$$

where d and L are the diameter and length of tube, and v_a is the average thermal velocity.

The gas flow from the center to the tube edge is $Q = [P(x) - P(0)]U(x)$, where

$$U(x) = \frac{\pi}{12} v_a \frac{d^3}{x} = \frac{U_0}{x}.$$

Neglecting the pressure on the tube edge P(0), one can write the pressure distribution over the tube as follows: $P(x) = Q/U(x) = Qx/U_0$.

Table 3

	σ_{-11} (cm^2)	σ_{01} (cm^2)	σ_{-10} (cm^2)	δ (cm^{-2})	E_{los} (eV)	ΔE_{los} (eV)
Nitrogen	0.47×10^{-16}	1.54×10^{-16}	3×10^{-16}	3.3×10^{16}	177.5	275
Magnesium	0.84×10^{-16}	1.26×10^{-16}	1.6×10^{-16}	3.9×10^{16}	306.6	406

The target thickness is

$$\delta = 2n\int_0^l P(x)\mathrm{d}x = 2n\int_0^l \frac{Qx\,\mathrm{d}x}{U_0} = 2\frac{nQ}{U_0}\frac{l^2}{2},$$

where $l = L/2$ is half of the tube length and n is the number of gas molecules in 1 cm^3 Torr.

So, the gas consumption necessary for the given target thickness is

$$Q = \frac{\delta U_0}{nl^2} = \frac{\delta U}{nl}.$$

Table 4 shows the values for Q and also for the pressure in the center $P(l)$ and on the output $P(0)$ of the tube at δ taken from Table 3.

The free path length at $P(l) = 3.8\times10^{-2}$ Torr for nitrogen is 1.7 mm at the effective size of 4 mm. The conductivity calculated for the molecular–viscous regime by the formula $U_{mv} = 0.9U + U_v$ [20] (where U_v is the conductivity for the viscous regime) differs slightly from U.

In a vacuum system, gas emission may also exist due to desorption of gas from the surface polluted with adsorbed gases, vapors, remaining water and oil films. Excluding the starting period of operation, the gas emission for polished stainless steel and ceramics is 3×10^{-9} l Torr cm^{-2} s^{-1} and 1.1×10^{-9} l Torr cm^{-2} s^{-1}, respectively [21]. With the whole square of the stainless-steel surface 2.8×10^5 cm^2 and ceramics 9.4×10^3 cm^2, the total gas emission from the walls is 1.1 cm^3 Torr s^{-1}. The value is expected to decrease in operation by hundred times.

3.2.3. Calculation of the vacuum system by the method of statistic tests

For the calculation of conductivity for components and pressure distribution in the vacuum system the method of statistic tests was employed (the Monte-Carlo method). With the statistic simulation of the gas flow in the vacuum system a large number of molecule trajectories are traced from the start to the moment of their return to the surface of the input or output or at the moment of saturation if there are saturating surfaces.

In the program used only molecular (collisionless) motion of particles is considered. This motion is characterized first of all by the linear trajectory, and second by the specificities in particle interactions with the vacuum chamber walls.

According to that mentioned above the mathematics simulation compresses two independent problems: the first one is the description of particle motion inside the vacuum cavity, and the second is the simulation of particle collision with the wall surface.

The first problem is solved in the following way: the particle motion is considered to be its simple motion from one point of the vacuum cavity surface to another along the direct line.

The particle collision with the surface of vacuum apparatus is characterized by (a) its probability to be absorbed, (b) probability of the isotopic (within 0–2π) reflection of particles. The simulation of the particle collision with the wall is performed with the Monte Carlo technique. Introduction of the surface properties is determined by giving the dependences of particle sorbtion probability, probability of the isotropic reflection of particles.

The probability for a molecule to fly out of the surface at the start or at the reflection according to the experimentally established cosine law is equal to: $\mathrm{d}P = \cos\gamma\,\mathrm{d}\omega/\pi$, where γ is an angle to the normal, $\mathrm{d}\omega = 2\pi\sin\gamma\,\mathrm{d}\gamma$ is an elementary solid angle. By the integration from 0 to 2π we get the fraction of molecules flying out inside the angle γ: $\xi = \int_0^\gamma \mathrm{d}P = \int_0^\gamma \sin 2\gamma\,\mathrm{d}\gamma = \sin^2\gamma$. Hence, the expression which is used for finding the random angle $\gamma = \arcsin\sqrt{\xi_1}$, at the generation by the random

Table 4

	N_2		Mg	
L (cm)	26	18	26	18
Q (cm^3 Torr s^{-1})	4.5	9.4	13.4	28.4
$P(l)$ (Torr)	3.8×10^{-2}	5.7×10^{-2}	6.8×10^{-2}	9.8×10^{-2}
$P(0)$ (Torr)	1.5×10^{-3}	3.1×10^{-3}	4.5×10^{-3}	9.4×10^{-3}

number transmitter uniformly distributed within the interval from 0 to 1, of the random number x_1. The random azimuthal angle φ is uniformly distributed within the interval from 0 to 2π: $\varphi = 2\pi\xi_2$.

The capability of the vacuum system component is defined by the probability of the shift of molecules from the input cross-section to the output one. For example, for the calculation of the charge-exchange tube capability it is assumed that both the input and output holes are the surfaces with the absorption coefficient 1. The injection surface is near the input surface and N particles are injected from the surface (the conductivity coefficient) is defined as $P = N_{out}/N$ were found as a result of calculations. In this case, the tube capacity is equal to: $U = U_0SP = U_0SN_{out}/N$, where U_0 is a capacity of 1 cm^2 hole (1.177×10^4 cm s^{-1} for nitrogen, 1.956×10 cm s^{-1} for magnesium at 400°C), S is the input hole area.

Fig. 10 shows various designs of the charge-exchange tubes with a 4 mm diameter of the input hole. The calculation results of the conductivities of these versions for nitrogen are given in Table 5. The calculation showed also the tube conductivity to be inversely proportional to their length, so by analogy with analytical calculation the usage of the tube with lowest conductivity will result in decrease of gas consumption by a factor of $(52.5/30.6) \approx 1.7$.

For finding out the pressure distribution in the vacuum system, the number of collisions (obtained in calculations) of molecules with the surface N_i referred to the surface area S_i is used: $P_i = KN_i/S_i$ where K is the coefficient. For the calculation in the vacuum system the pump input pressure is $P_p = Q/V_p = 2.25\times10^{-6}$ Torr, where $Q = 4.5$ cm^3 Torr s^{-1} is the gas emission in the system, $V_p = 2$ m^3 s^{-1} is the pump rate. If the number of collisions with the surface S_p is equal to N_p, $K = P_pS_p/N_p$. With a single pump in the system all injected particles N are absorbed by the surface S_p, and the number of collisions is $N_p = N/f$, where f is the vacuum factor of the pump, and $K = fP_pS_p/N$.

The pressure distribution in the vacuum system at the given values is shown in Fig. 11. The gas flow from the gas charge-exchange tube enters mostly to the upper large holes. A and B partitions with the holes of 5 and 6 mm protect the acceleration tract from gas. Calculation shows that in the tract area the pressure exceeds the one shown in the draft less than 10^{-7} Torr.

4. Power high-voltage source of accelerator for generation of neutrons for NCT and FNT

In this project the high-voltage rectifier of ELV-type accelerators which are used for industrial application are offered for use as the high-voltage source.

Before looking at the high-voltage source we will be concerned with the main parameters of ELV-type accelerators and their construction features which can be used when the accelerator for neutron generation will be made.

4.1. Main parameters of ELV-accelerators

Beginning from 1971, BINP started its activity in the development and manufacturing of electron accelerators of the ELV type for their use in industrial and research radiation–technological installations [22]. The ELV-type accelerators are designed with the use of the unified systems and

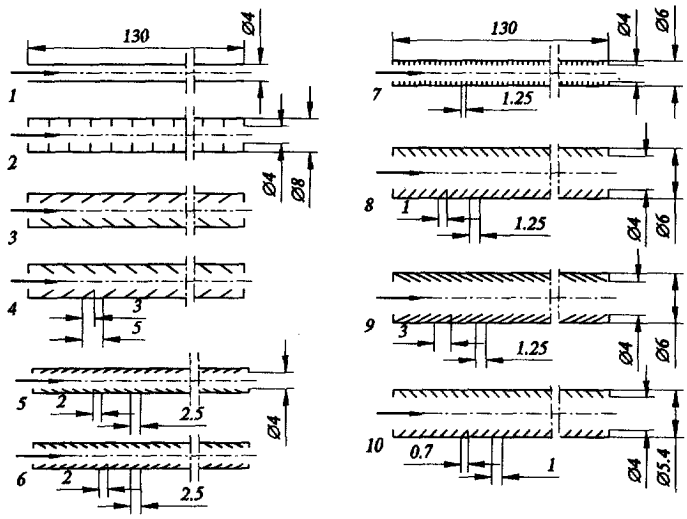

Fig. 10. Designs of the change-exchange tubes, have ring partitions (1–7 - in scale 1 : 1, 8–10 - in scale 2 : 1). Arrows indicate the place of particles injection.

Table 5

No. designs	1*	1	2	3	4	5	6	7	8	9	10
U ($cm^3\ s^{-1}$)	60.6	52.5	61.2	68.0	59.4	60.2	46.3	38.5	35.1	43.1	30.6

*For comparison, in the first column of table there is the conductivity value for the first version calculated by the analytical formulae.

units enabling thus to adapt them to the specific requirements of the customer. The design and schematic solutions provide the long-term and round-the-clock operation of accelerators under the conditions of industrial production processes. The specific features of the ELV-accelerators are the simplicity of design, convenience and ease in control and reliability in operation.

BINP proposes a series of electron accelerators of the ELV-type covering the energy range from 0.2 to 2.5 MeV with a beam of accelerated electrons of up to 200 mA and maximum power of up to 160 kW. By now, over 70 accelerators have been delivered inside our country and abroad and the total operation time exceeds 500 accelerator years. Basic parameters of the ELV-type accelerators are given below (Table 6):

Apparently from the table the high-voltage rectifiers of our accelerators by its parameters (energy and power) can be used for NCT and FNT purposes.

General view of the ELV-type accelerator with a foil extraction is given in Fig. 12 and Fig. 13. Inside the tank filled with the SF_6 gas the primary winding, the high-voltage rectifier with a built-in accelerating tube, high-voltage electrode and the injector control unit are located. Just the location of the accelerating tube inside the column of the high-voltage rectifier makes the ELV-accelerators the most compact among the devices of this class. The vacuum system components and extraction device are fixed to the bottom of the tank. But they will not be used for the purpose of neutrons generations.

The source of high voltage is a cascade generator with a parallel inductive coupling. The rectifier section column is installed inside the primary winding. The rectifying sections are connected in series.

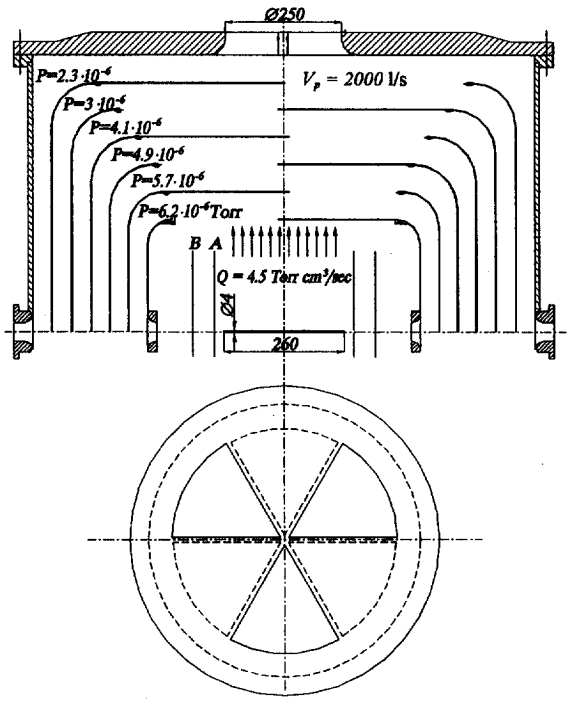

Fig. 11. Distribution of pressure in the vacuum system at $Q = 4.5\ \mathrm{cm^3\ Torr\ s^{-1}}$.

The rectifier section column is terminated with the high-voltage electrode. The use of the low inductive ceramic capacitors, original scheme of intersection connections, and the presence of damping resistors provide the reliable protection of components of high-voltage rectifier against the overvoltages during break-downs both of vacuum and gas insulation. The practice proved the high reliability of the high-voltage rectifier.

4.2. *High-voltage source for NCT and FNT*

The high-voltage sources of the ELV-4, ELV-6 accelerator (tandem version) and ELV-8 accelerator (direct accelerating of protons version) with changing polarity of output voltage are the most convenient.

For tandem version the ELV-4 accelerator rectifier can provide proton beam current up to 20 mA. It corresponds to full power 40 kW. If one wants to increase the proton beam current up to 50 mA, (i.e. full current rectifier 100 mA), one should use the ELV-6 accelerator. The use of high-voltage sources of ELV-8, will be useful for direct (without recharging) acceleration of protons. In this case the max. proton's current is equal to 50 mA.

Table 6

	Energy range (MeV)	Beam power (kW)	Max. beam current (mA)
ELV-mini	0.2–0.4	20	50
ELV-0.5	0.4–0.7	25	40
ELV-1	0.4–0.8	25	40
ELV-2	0.8–1.5	20	25
ELV-3	0.5–0.7	50	100
ELV-4	1.0–1.5	50	100
ELV-6	0.8–1.2	100	100
ELV-8	1.0–2.5	90	50
ELV-6M	0.75–0.95	160	200
Torch	0.5–0.8	500	800
ELV-12	0.6–1.0	400	400

The energy stabilization system of ELV-type accelerators provides 1–2% instability of accelerating voltage. The value of voltage ripples is about 10 kV. These parameters are acceptable if the high-voltage source is used for the production of FNT neutrons. However, for NCT neutrons the instability of accelerating voltage should be no more than 0.1%, and the stabilization system should be modified. For this purpose:

it is necessary to design a slow feedback of stabilization based on precise measurement of the accelerating voltage and the accelerated proton energy. The usual resistive divider of ELV accelerators cannot provide the required accuracy and stability of measurements. So we should use for precise measurements the divider with the special microwire resistors or high-accuracy-generating voltmeter and low current beam of neutrals (that should be additionally stripped) after the parallel shift system of proton beam (see Section 2). Two independent systems allow to obtain the instability of accelerated proton energy average level less than 10^{-3};

it is necessary to design the system for active suppression of high-voltage source ripples with a strip range equal to a few kHz. The signal from

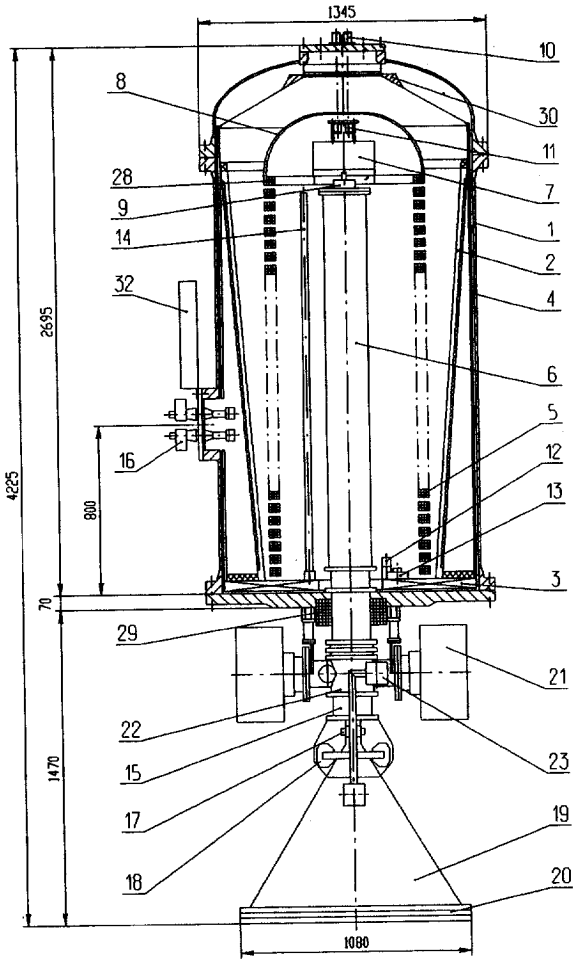

Fig. 12. General view of ELV-4 accelerator: (1) vessel, (2) primary winding; (3,4) magnetoguides; (5) rectifier sections; (6) accelerating tube; (7) injector control unit; (8) high-voltage electrode; (9) injector; (10,11) optical channels for injector control; (12) section divider; (13) capacitor unit; (14) energy divider; (15) vacuum gate; (16) primary winding terminals; (17,18) scanning coils; (19) extraction device; (20) extraction window frame; (21) vacuum pumps; (22) cross head; (23) vacuum gate; (28) base of high-voltage electrode; (29) magnetic lens; (30) high-voltage shield; (32) clamp set.

the capacitance probe will produce the compensating voltage. The compensating signal will pass from ground to the high-voltage terminal through the capacitors of the rectifier column. This system will provide the stability of the protons energy during the short-time interval.

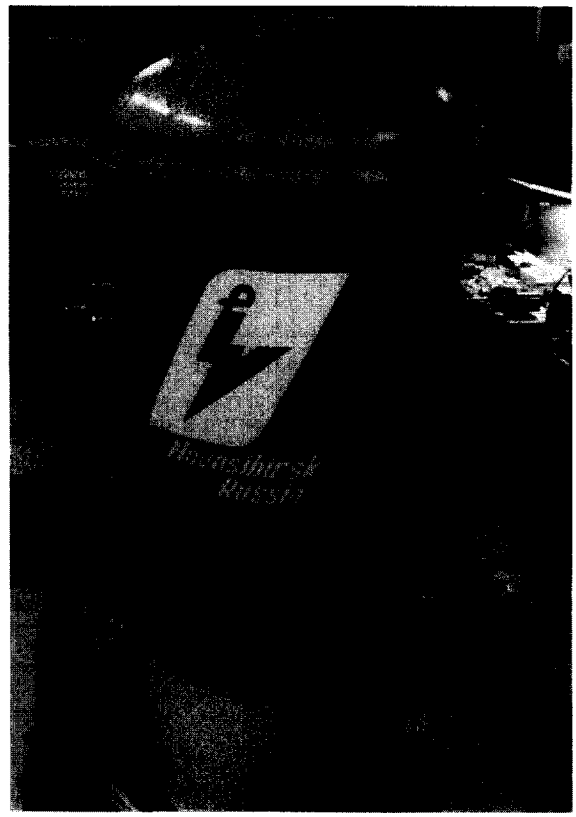

Fig. 13. Photo of the accelerator ELV-8.

Parallel operation of the both systems allow to obtain required stability of energy. Now we develop the system of stabilization for a powerful source with output voltage 600–800 kV and instabilities 200–300 V.

4.3. Control system

The control system for the high-voltage power source is practically the same as one of the industrial accelerators. The operator communicates with the accelerator through the computer. The accelerator control system comprises a set of software and hardware covering all the accelerator units required an operative control and diagnostics. The multifunctional control system enables one:

- to make the automated control of the accelerator. Algorithms introduced into the accelerator

control program, solve the problems from the preparation of the accelerator to its operation, watches the status of blockings before and, after switching on, of the accelerator and installs an energy and current of an accelerator in the given regime;
- to stabilize safely the main parameters of an accelerator;
- to provide the continuous diagnostics of the high-voltage rectifier and self-testing of the other systems during the operation of accelerator;
- to synchronize the accelerator operation and technological equipment;
- and provides for the personnel a wide choice of commands for the regimes of testing and adjusting the accelerator to be preliminary issued.

The software of the accelerator control system provides a friendly interface with the user through the system of dynamic menus, text and graphic visualization of the accelerator operation run.

4.4. Power supply system

The power supply of the primary winding of the high-voltage rectifier is provided by the frequency of 400–1000 Hz from the frequency convertor. The total efficiency is 65–80% for rotating (motor-generator) and 85–92% for static (thyristor or transistor) frequency convertors.

All the operative reswitching in the power supply cabinet is made by the control program automatically without actions of the operator. The power system is not needed in the changes when it works in a complex for generation of the neutrons.

5. The steady-state H^- ion source with a beam current of up to 40 mA

For a tandem proton accelerator for neutron generation, intended reliably to work in hospitals, it is necessary to create a steady-state reliable source of negative hydrogen ions with a long operation lifetime. The source should permit to obtain a H^- ion beam with a relatively small emittance and with a steady-state ion current of some tens of milliamperes, as it appear, not more than 40 mA.

To satisfy these requirements, outcoming from our and world experience, we have chosen a surface-plasma source (SPS) in a multicusp geometry with a cesiated spherical emitter of H^- ions (a convertor). A schematic diagram of the ion source is shown in Fig. 14. It consists of a gas-discharge chamber with an internal diameter of about 12 cm and height of about 8 cm. Samarium–cobalt magnetized rods surround the chamber as shown in the figure. They form a multicusp "magnetic" wall of the discharge chamber. The multicusp magnetic wall will be optimized to improve a discharge plasma confinement in the final ion source design.

Hydrogen will be injected to the chamber through thin channels in the H^- ion emitter, as it is shown in Fig. 14. The discharge plasma in the chamber will be produced by an electron flux with an energy of 30–60 eV from LaB_6 cathodes. One or two cathodes will be installed in the chamber through a cylindrical wall. The LaB_6 cathode with a diameter of an emitting surface of 18 mm permits to get the 15 A electron current with a cathode lifetime of not less 2000 h and 30 A with a lifetime of 500 h. The design and technology of such cathodes are developed in BINP [23]. We suppose, that a 15–30 A electron current will be sufficient for ionization of hydrogen in the chamber with good magnetic walls. The Mo-emitter of H^- ions will have a negative potential of about 100 V relative to the chamber and will be bombarded by plasma hydrogen ions. Adsorbed hydrogen atoms will be knocked off and atomic fragments of dropping ions will be reflected from an emitter surface.

A cesium vapor will come to the emitter surface through thin channels in it, as it is shown in Fig. 14. Cesium will cover the emitter surface owing to its diffusion on the surface, as a result of ionization of the cesium vapor injected from channels with a subsequent return of cesium ions by an electrical field to the surface. For the considerable reduction of the cesium condensation on the chamber walls, the hot thin metal shield will be used. A monolayer coverage on the H^- ion emitter surface will be produced at a cesium rate of few 1 mg h^{-1}. Thus, the work function of the surface is reduced down to 1.5 eV. Due to the low work function fast desorbed and reflected hydrogen atoms with an electron affinity

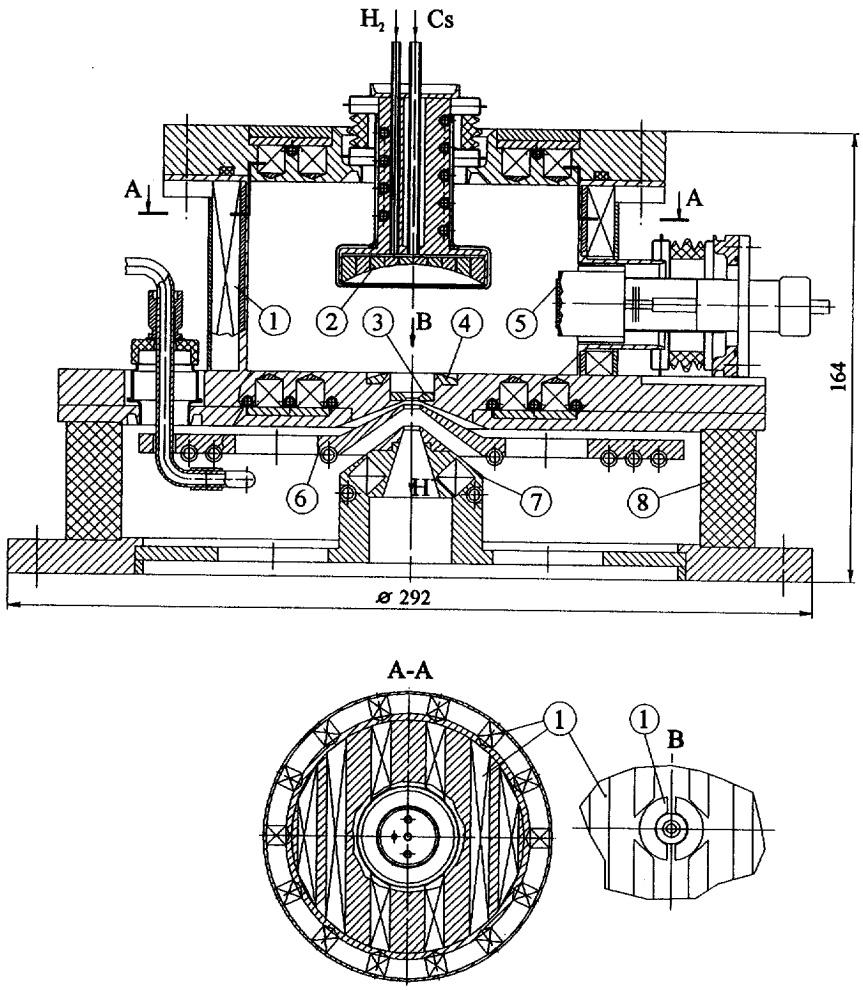

Fig. 14. H^- ion source. (1) "magnetic" wall of gas-discharge chamber, (2) emitter of H^- ions, (3) plasma electrode with outlet hole, (4) magnetic filter of electrons, (5) LaB_6 cathode, (6) extractor, (7) accelerating electrode, (8) 30 kV main insulator.

of 0.75 eV leave the emitter surface as H^- ions with a probability close to an unity. The H^- ion emitter is a cold cathode with a high secondary ion-electron emission coefficient. The electron current from the emitter will be added to one from the hot LaB_6 cathodes. This can increase the ionization of hydrogen in the chamber. The H^- ions are accelerated by a near-electrode potential drop and are focused into an emission aperture on the anode wall of the chamber (3, Fig. 14). Thus not all H^- ions leaving the emitter pass through the emission aperture.

The considered H^- emitter potential (about to -100 V) allows us to convert hydrogen particles from plasma into H^- ions quite efficiently under significant limitation of cesium consumption [24–30].

On the basis of work experience with SPS in a similar geometry developed in LBL [31], we expect that at a hydrogen pressure of not higher than 1 mTorr in the discharge chamber the stationary plasma with electron density of the order of 10^{12} cm^{-3} will be obtained. The minimum ion

temperature is 0.1 eV. The hydrogen ion species ration of plasma depends on the hydrogen pressure and at the pressure of 1 mTorr ions are basically molecular (H_2^+, H_3^+) [32]. The appropriate current density of hydrogen atomic particles to the surface will not be less than 0.1 A cm^{-2}, and the current to the 20 cm^2 emitter surface will be not less than 2 A. Thus, about 400 mA of H^- ions will be emitted from the cesiated emitter surface [28,29,32].

The 100 eV H^- ions from the spherical emitter are focused into the emission aperture with a diameter of 0.5 cm on the anode. At a 5 cm distance from the emitter to the emission aperture only H^- ions emitted with an mean angular spread of $\pm 2.5°$ will pass the emission aperture. The mean angular spread of ions emitted from the surface is approximately $\pm 5°$. From here it follows that approximately 25% of the H^- ion flux emitted from the convertor pass through the emission aperture. The H^- ions in motion to the emission aperture will be lost by gas and plasma. The main processes of H^- loss are:

$$H^- + H_2 \rightarrow H_0 + \cdots,$$

$$H^- + H^+, H_2^+, H_3^+ \rightarrow H_0 + \cdots,$$

$$H^- + e \rightarrow H_0 + 2e.$$

Because of the mentioned losses of H^- ions their flux from the emitter can be reduced by approximately 30%. As a result about 18% of emitted ions or about 70 mA can pass the emission aperture.

The H^- ion beam from the emission aperture is accelerated up to 25 keV and moves in hydrogen flowing from the emission aperture. Thus the initial mean free path of H^- ions because of their loss by hydrogen is 30 cm. On account of the divergence of outflowing hydrogen, 10–15% of H^- ions will be lost. Based on this, according to estimations some reserve from the H^- ion current is required.

For the formation and acceleration of the H^- ion beam the three-electrode ion-optic system (IOS) is provided: a plasma electrode (3, Fig. 14), an extractor (6) and accelerating electrode (7). The plasma and accelerating electrodes have Mo-insertions. According to a space charge of the emitted H^- ion beam with the current about of 50 mA the total gap in the IOS should be 9 mm. For reduction of an accompanying electron flux a magnetic filter (a local cross magnetic field over the emission aperture) is provided. In the IOS gaps a small counter cross magnetic field is formed, convex to the emission aperture. The electrons passed through the emission aperture are dumped along the convex magnetic field to the copper extractor. At allowable heating of a near-beam edge of the copper electrode up to 500°C it is possible to dump electrons with a power of up to 600 W (200 mA at extracting voltage 3 kV). In order to compensate the deflection of the H^- ions inside the electron magnetic filter, the position of the convertor will be corrected [33].

A vacuum chamber, through which the H^- ion source is connected to the tandem accelerator, is shown in Fig. 15. The chamber is the two-volume cylindrical vacuum chamber with a diameter of 0.5 m, a total length of about 1 m and with a horizontal axis being in line with an axis of the tandem accelerating column.

The H^- ion source (1, Fig. 15) is connected above to a cylindrical wall of the first volume (2) with the length of 0.6 m. The H^- ion beam enters the chamber from the top along a vertical, is turned 90° by a separating magnet, passes along a horizontal through a small aperture (9) in the wall into the second volume (3), intersects along the axis the second volume and is injected into the tandem accelerating column (14).

The H^- ion beam with the current 40 mA has a large enough space charge density and requires along a transport path from the ion source to the tandem accelerator a strong enough nearly continuous focusing. In front of the tandem entrance it is necessary to have a large spread of the beam with a minimum focal distance of 5 cm from an initial point at a distance of 11 cm from an external potential surface of the tandem accelerator. It is connected with a large force of an inlet lens formed by a field of the accelerator at the entrance. To satisfy the mentioned conditions of injection of the ion beam into the tandem accelerator it is provided to abruptly focus the beam at the initial point (at 11 cm from the entrance) by a pair of single electrostatic lenses (7,8) with a large aperture (maximal diameter of the beam in the lenses is $\approx$ 4–5 cm). This pair of the lenses ensures an ion-optical

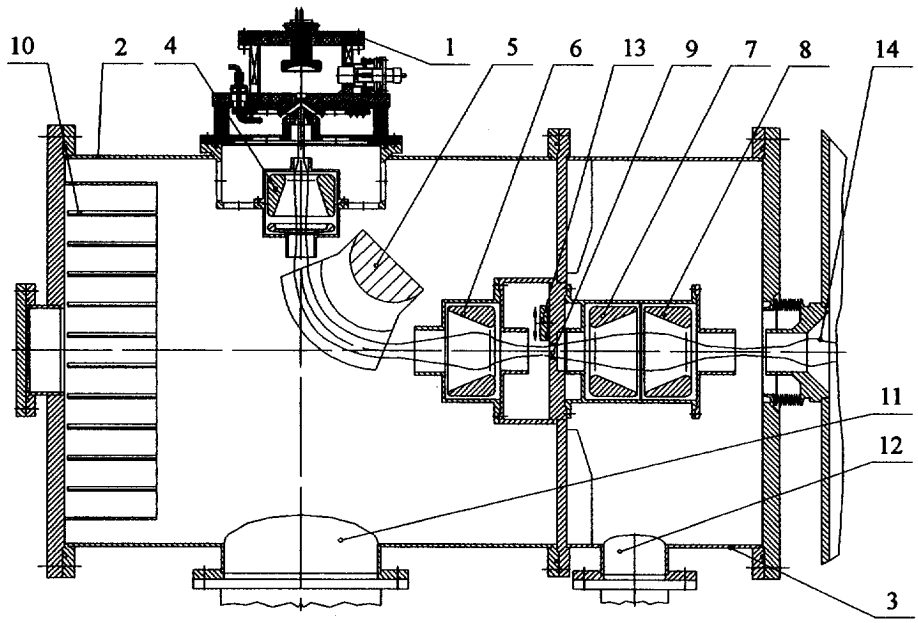

Fig. 15. Chamber of H^- ion source. (1) H^- ion source, (2) 1st volume, (3) 2nd volume, (4, 6, 7, 8) electrostatic lenses, (5) separating (bending) magnet, (9) inter-volume aperture, (10) shelves with zirconium powder, (11, 12) holes for turbomolecular pumps, (13) vacuum valve, (14) entrance into tandem accelerator.

matching in the second volume, which is adjacent to the tandem accelerator.

The separating magnet (5) with two single electrostatic lenses installed before (4) and after (6) the magnet is located in the first volume. The H^- ion beam passes in the IOS the first 7 cm of the path in a compensated state, as far as in this area the density of the gas, flowing from the source, is high enough.

At the inlet into the first single lens the beam is decompensated and further focusing is accomplished by single lenses and the separating (bending) magnet. At the entrance into the second volume the beam is compressed with its diameter down to 1.5–2 cm. It passes through the 2 cm-in-diam aperture in a diaphragm between the volumes.

At the 1 mTorr hydrogen pressure in the source through the emission aperture with diameter of 5 mm the hydrogen flow of about 10^{-2} l Torr s^{-1} enters the first volume. For the maintenance of vacuum in the first volume with the pressure of 10^{-5} Torr, the pumping rate of 1000 l s^{-1} is necessary. Below the first volume a hole (11) with a diameter of 200 mm for connecting a 1000 l s^{-1} turbo-molecular pump is stipulated. The hydrogen flow 10^{-3} l Torr s^{-1} is injected into the second volume through the aperture in the diaphragm. A hole (12) with a diameter of 100 mm for connecting a 550 l s^{-1} turbo-molecular pump is stipulated below the second volume. The pumping of the second volume by this pump allows to maintain a vacuum of 10^{-6} Torr.

From the H^- ion source, cesium will be injected into the first volume in a quantity of a few mg $hour^{-1}$ or 5–10 gy^{-1} at daily operation during 10 h. For absorption of cesium in the first volume on special shelves (10) zirconium powder with grains of diameter 0.1 μm is located [34]. Zirconium has a high adsorption energy for Cs atom: 3.22 eV for a zero coverage and 2.55 eV for a monolayer. One litre of the powder at the monolayer Cs coverage of grains can absorb more than 15 g of cesium. Thus it is enough to place into the first volume 0.5 l (≈2 kg) of the powder to ensure the

absorption of cesium during one year of the operation approximately. A replacement of the powder can be made within some hours. The pressure of saturated cesium vapors for the Cs monolayer on zirconium is formally equal to zero. Therefore, it is important only to prevent a direct hit of Cs atoms from the first volume to the second volume through the aperture in the diaphragm.

Another way of removal of cesium is to establish a freon refrigerator and to cool special plates down to $-30°C$ [35]. Thus, the pressure of saturated cesium vapors in the first volume will not exceed 10^{-9} Torr.

We note that surface-plasma sources with using cesium operate for many years on largest accelerators of the world. So magnetron-type SPSs operate from 1977 on accelerators in the laboratories of FNAL, BNL, ANL, DESY, Ratherford [36]. In majority of cases they were installed on Cockroft–Walter preinjectors with a stationary voltage of 750 kV. No influence of cesium from SPS on an electric strength of accelerators was observed. The offered multicusp type of SPS is similar to the one used for many years on accelerators in laboratories of LANL [37] and KEK [38]. In LANL such a source has been operating from 1985 with a small duty factor: at the nominal current in a pulse of 20 mA the mean H^- ion current is 2 mA.

The separating magnet with a 3 cm gap between poles is designed with the use of samarium–cobalt insertions. For the beam energy of 25 keV the product of the field by the turn radius is about 23 kGs cm. The turn radius is 12 cm. The appropriate magnetic field on the transport path is 1.91 kGs. The magnetic field of the samarium–cobalt magnet is varied 3×10^{-4} at a 1° temperature variation. Since the turn angle should be kept accurate to within 10^{-3}, the magnet temperature should be stabilized by cooling water with variation of its temperature within $\pm 3°$. On the diaphragm between the first and second volumes a small vacuum valve (13, Fig. 15) is provided which can close hermetically the aperture with a diameter of 2 cm. Due to this, without leaking the atmosphere into the tandem accelerator, one can leak the atmosphere into the first volume and replace the source cathodes, replace the zirconium powder and perform preventive maintenance of the ion source and ion-optic elements. It should be emphasized that the only dry air should be leaked into the first volume to avoid a CsOH formation on walls. A harmless Cs_2O is formed at the leak-in of the dry air. A periodic leak-in of the dry air permits "to destroy" a metallic cesium in the vacuum chamber. After the atmosphere leak-in 3–5 h is required for the conditioning of the H^- ion source. If the source cathodes have a operation lifetime of 2000 h, this operation has to be conducted twice a year.

6. Neutron-producing lithium targets

This project envisages a possibility of operation in two regimes of neutron generation – obtaining fast neutrons at an energy of a proton beam of 2.5 MeV during the formation of the necessary neutron spectrum with the use of the moderator and the operation near the threshold of the reaction $^7Li(p,n)^7Be$ at the proton energy of 1.885 MeV providing the generation of directed beam of neutrons with quite narrow spectrum at medium energy of ~ 30 keV. Therefore, it is desirable that the target design could be applicable to both these versions.

Since at 2 MeV the protons range in lithium is ~ 0.3 mm the target can be made in the form of a hard well cooled plate placed in vacuum, one side of which faces the incident beam is coated with a thin layer of lithium which is the target. If the lithium moistens well the sublayer material, its thickness will be of a few tenths of a fraction of a millimeter and such a target can operate at temperatures above the lithium melting point. The limit of target temperature will be the pressure of saturating P_{sat} lithium vapors increasing fast with temperature (Table 7). Dependence of lithium evaporation rate V_{ev} on temperature is also shown in Table 7.

Therefore, the operation at temperature above 400°C is undesirable since it leads to complications in pumping and to large consumption of lithium. The target design is given in Fig. 16.

It is a tungsten disk (1) in the form of a "plate" with 2 mm thick bottom. The inner surface of the

"plate" is covered (moistened) by a thin layer of lithium (2). On the outer side of the "plate" the rectangular grooves 1 mm deep and 3 mm wide (3) are covered by a 0.1 mm thick molybdenum foil (4). The foil is welded to the tungsten disk by diffusional welding so that in the target bottom the narrow channels are made for cooling. At the end of each channel, there are round holes (5) connecting them to the collector cavities (6) made in the form of concentric half-rings in the thick tantalum ring (7) also welded to tungsten by diffusional welding.

Each narrow channel is connected in turn either from the inner or outer collector cavity that enables the passage of cooling liquid along the neighboring channels in opposite directions. The cooling liquid is applied to the opposite sides of the target disk through the pair of coaxial tubes (9) of which the outer tube is welded to the collector ring and the inner one is just tightly inserted into the outer tube. The feeding tubes are connected with the copper packings (10) to the collecting disk. The packing is provided by two lever clamps (11) so that the target can easily be connected to the body (14) after coating with lithium and testing on the special vacuum stand. After connecting the target it is covered with a vacuum chamber (12) closed at the end by a thin molybdenum foil (13). The chamber has a view glass window (8) on its side cylindrical surface for the observation of the condition of the lithium surface and electric inputs (not shown in the figure) for the connection of thermal pairs measuring the temperature of the inner (lithium) and the outer surfaces of the target. From above, to the body the long vacuum tube (16) is connected through which the pumping and dropping of the proton beam onto the target is performed. On the inner surface of vacuum tube, is the system of cone diaphragm-catchers of molecules of evaporating lithium (17). The cooling liquid is supplied to the target device through the feeding tubes (15), connecting it to the pump and heat exchangers.

6.1. Thermal regime of the target

The neutron generating target will be operated in the very complicated thermal regimes. At the proton energy of 2 MeV and an average beam current of 10 mA the power produced on the target surface will be 20 kW. At a beam diameter of 5 cm, the cooling made through the thin tungsten layer, should provide the evacuation of heat flux with density $q = 1\ \mathrm{kW\ cm^{-2}}$.

The considered design enables the cooling of the target by any cooling liquid. Let us compare the cooling efficiency by water and by liquid metals – Gallium ($T_m \approx 30°C$) and mercury. If the temperature distribution over the lithium thickness $h_{Li} \approx 0.3$ mm is assumed to be homogeneous (absorbtion length of 2 MeV protons in lithium is ~ 0.3 mm), its average temperature can be evaluated as $T_{Li} \approx \Delta T_w + \Delta T_{w-liq} + T_{liq}$, where ΔT_w is the temperature drop on the tungsten wall, $\Delta T_{w-liq} = T_w - T_{liq}$ is the difference of temperatures of the cooling tungsten wall and liquid; T_{liq} is the temperature of the cooling liquid. The temperature drop on tungsten can be estimated as $\Delta T_w = q\, h_w/\lambda_w$, where h_w is the tungsten wall thickness, λ_w is the tungsten heat conductivity. The tungsten has the best heat conductivity among metals (except for silver, copper, gold) $\lambda_w \cong 1.3\ \mathrm{W\ cm^{-2}\ degree^{-1}}$ within the temperature range 20–300°C. At $q = 1\ \mathrm{kW\ cm^{-2}}$ and $h_w =$ 1 mm, $\Delta T_w = 80°$ and it is independent of the kind of cooling liquid. The heating of liquid upon its passage of cooling channel will be determined by its rate of flow $P = S \cdot V$ (S is the channel cross-section, V the liquid velocity) and by the thermal capacity. At our geometry ($S = 3 \times 1\ \mathrm{mm^2}$), at the velocity of $V = 10\ \mathrm{m\ s^{-1}}$, the rate of flow will be $P = 30\ \mathrm{cm^3\ s^{-1}}$ and the maximum output temperature $T = q/C_p \gamma P$, where γ is the density, C_p is a mass thermal capacity. The liquid heating is: H_2O – $T_{liq} = 16°$, Ga – $T_{liq} = 30°$, Hg – $T_{liq} = 35°$.

Table 7

T (°C)	180	204	234	268	306	350	390	450	520
P_{sat} (Torr)	10^{-10}	10^{-9}	10^{-8}	10^{-7}	10^{-6}	10^{-5}	10^{-4}	10^{-3}	10^{-2}
V_{ev} (g cm^{-2} h^{-1})	3.4×10^{-9}	3.4×10^{-8}	3.4×10^{-7}	3.4×10^{-6}	3.4×10^{-5}	3.4×10^{-4}	3.4×10^{-3}	0.034	0.34

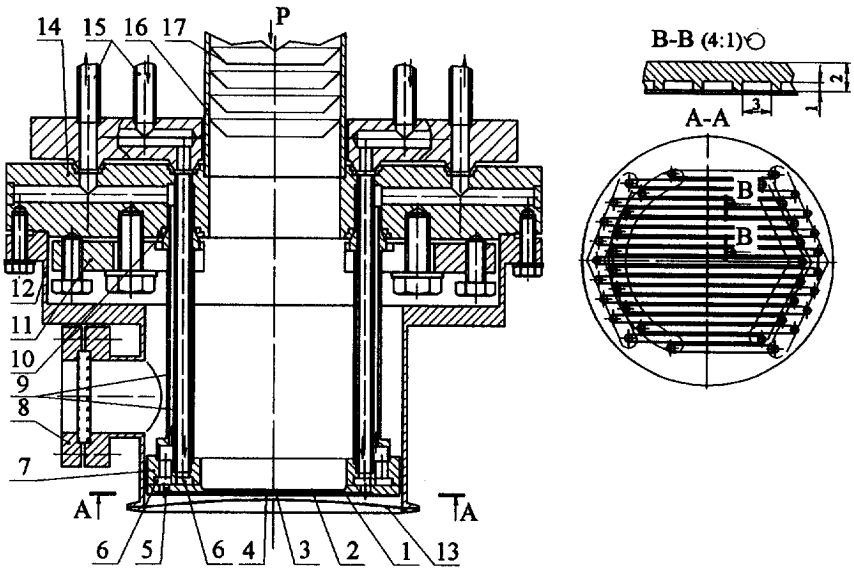

Fig. 16. Neutron generating lithium target. (1) tungsten disk; (2) lithium layer; (3) cooling channels; (4) tantalum foil; (5) feeding holes; (6) collector cavities; (7) tantalum ring; (8) observing window; (9) feeding coaxial tubes; (10) copper packings; (11) lever clamps; (12) vacuum chamber; (13) molybdenum foil; (14) body; (15) heat carrier feeding tubes; (16) vacuum chamber; (17) cone catchers of lithium vapors.

A more complicated thermodynamic process determines the temperature drop between the cooled wall and heat carrier which at the convective heat exchange is expressed as $\Delta T_{w-liq} = q/\varepsilon$, where ε is the heat transfer factor which is determined by the hydrodynamic regime of liquid flow and by its thermodynamic properties.

For the effective cooling one has to provide the turbulent flow of liquid when the Reynold's number $Re = Vd_r/v$ exceeds the critical value $Re > Re_{cr} = 2300$. Here V is the liquid velocity, v ($m^2\ s^{-1}$) the kinematics factor of liquid viscosity and d_r is the characteristic transverse size of the channel. With the rectangular channel, $d_r = 4S/\Pi$, S is the channel cross-sectional area, Π is its circumference (in our geometry, $d_r = 1.5$ mm).

The heat transfer coefficient is defined as $\varepsilon = N\lambda/d_r$. Here Nu is the Nusselt criterion defined by the empirical expression (critical equation): $Nu \approx 0.023Re^{0.8}\ Pr^{0.4}$, $Pr = v \cdot C_p \cdot \gamma/\lambda$ is the Prandtl criterion. For the liquid-metal heat carriers (Prandtl criterion $Pr \gg 1$) by computing the efficient value of the Nusselt criterion one has to introduce the correction presented in terms of Peckle criterion [39] as $Pe = Re\ Pr$: $Nu_{eff} = Nu + 0.044Pe^{0.75}$.

The main values determining the values of criteria Re, Pr and Pe are given in Table 8.

For water, the Prandtl criterion is much larger than that for metals and it strongly depends on temperature: H_2O: Pr = 7 for $T = 20°C$ and Pr = 3.1 for $T = 60°C$; Ga: Pr = 0.016; Hg: Pr = 0.016.

The heat transfer coefficient ε is strongly dependent on the heat carrier velocity V ($Re \sim V$). The choice of V is determined by the accessible consumption of the heat carrier and by the hydrodynamic pressure drop when flowing through the channel which is defined as follows:

$$\Delta P = \varepsilon \frac{l_k}{d_r} \frac{V^2}{2g} \gamma,$$

where $\varepsilon = 0.025$ for water. For water in our geometry at the velocity $V = 10\ m\ s^{-1}$, $P \approx 0.5\ kg\ cm^{-2}$, so that higher velocities $V > 10\ m\ s^{-1}$ can also be considered. Table 9 shows the computation results for $T_{w\text{-}liq}$ at $q = 1\ kW\ cm^{-2}$ for various heat carriers at different velocities and the heat

Table 8

	γ (kg/m^3)	λ (W m^{-1} degree^{-1})	C_p (J kg^{-1} degree^{-1})	ν (m^2 s^{-1})
H_2O	10^3	0.65	4.2×10^3	1×10^{-6} (20°C) 0.47×10^{-6} (60°C) 0.2×10^{-6} (100°C)
Ga	6×10^3	27	0.37×10^3	0.2×10^{-6}
Hg	13.6×10^3	9.5 (100°C)	0.14×10^3	0.1×10^{-6} (100°C)

Table 9

	V (m s^{-1})	1	5	10	15	20
H_2O	P (kg cm^{-2})		0.15	0.6	1.3	2.3
	$\Delta T_{w\text{-}liq}$ (°)	600	270	160	110	90
	T_{liq} (°C)	160	32	16	11	
Ga	P (kg cm^{-2})	0.04	0.9	3.5	7.8	
	$\Delta T_{w\text{-}liq}$ (°)	60	46	35	29	
	T_{liq} (°C)	300	60	30	20	
Hg	P (kg cm^{-2})	0.08	2	8		
	$\Delta T_{w\text{-}liq}$ (°)	60	48	37	8	
	T_{liq} (°C)	350	70	35	23	

carrier temperature and pressure drop, respectively, when flowing through the cooling channel.

It is seen that with water cooling the main contribution into the lithium layer temperature $T_{Li} \approx \Delta T_w + \Delta T_{w\text{-}liq} + T_{liq}$, is provided by the temperature drop between the cooling surface and heat carrier. Even at water velocity of 15–20 m s^{-1}, in practice, T_{Li} reaches the melting temperature $T_m = 186$°C. With an account for the non-uniform distribution of beam density and temperature drop over the lithium depth its surface will apparently be melted. An increase in water rate over 20 m s^{-1} is ineffective because of the non-linear dependence of $\Delta T_{w\text{-}liq}$ on V. Thus, the water cooling seems to be satisfactory at the proton beam current value not exceeding 10 mA ($q = 1$ kW cm^{-2}). In the case of increase in current up to 20–40 mA, one has to shift to the liquid-metal heat carriers. In this case, the cooling of tungsten surface will not be limited by the temperature drop between its surface and the cooling liquid $\Delta T_{w\text{-}liq}$ but the temperature drop over its thickness $\Delta T_w \sim q$ (at $h_w = 1$ mm, $q = 1$ kW cm^{-2}, $\Delta T_w = 80°$) will be the limiting factor. Therefore, it is desirable to decrease the tungsten surface thickness down to fractions of a millimeter. At the operation with melted lithium at temperature $T_{Li} \leq 350$°C in the geometry under consideration, one can provide the cooling of the target by gallium up to current values of 40 mA.

Such mode of work with the increasing of heat flux density to $q = 4$ kW cm^{-2}, probably, should be considered as hardly feasible. As a reserve, a compromise variant with the increasing of targets surface up 10 cm in diameter with the corresponding decreasing of q may be considered. However, it results in the decrease of the neutron flux density – especially undesirable in works in the near-threshold region without an external collimator. It is also necessary to bear in mind that with current of proton beam 40 mA full power releasing in the target will reach 100 kW – it essentially complicates the liquid lithium heat carrier pumping system and heat exchanger.

It was proposed in a previous consideration that all the power of the proton beam is released in the infinitely thin lithium layer. With finite thickness of

lithium layer h_{Li} and uniform distribution of releasing power the temperature drop on lithium will be $\Delta T_{Li} = qh_{Li}/2\lambda_{Li}$. Heat conductivity of lithium is significantly less than the tungsten one $\lambda_{Li} = 0.53\ W\ cm^{-2}\ degree^{-1}$, so that with $q = 1\ kW\ cm^{-2}$ and thickness of lithium layer $h_{Li} = 0.3$ mm – the absorption length of 2.5 MeV protons, – the temperature drop will be $\Delta T_{Li} = 28°$. If the thickness of the lithium layer is more than the protons path then the temperature drop on additional lithium layer will be $\Delta T_{Li} = qh_{Li}/\lambda_{Li}$ with full thickness, for example, $h_{Li} = 1$ mm will be $\Delta T_{Li} = 160°$. That is why the desire to minimize the thickness of target to $h_{Li} \leq 0.1$ mm, thickness where the effective neutron generation process have place, is caused only by requirements of heat removal.

Creation of such liquid-lithium target and control of its thickness during long operations in conditions of evaporation will be one of the technologically complicated problems while designing the target.

It is proposed to get thin lithium layers on the surface of tungsten disk by means of evaporation. A variant of special lithium vaporizer situated directly in target device (not shown in Fig. 16) (Fig. 17) and realizing evaporation of lithium continuously (or periodically switched) on the surface of target during operation, is considered. Thereby, necessary thickness of the liquid-lithium layer will be kept and controlled, for example, by value of neutron-flux. If the temperature of the target exceeds 300°C then there appears a problem of pumping out of lithium vapors and of periodical cleaning of the vacuum-guide surface in the target region from absorbed lithium.

For the horizontal proton beam the other variant of liquid-lithium target is considered – in the form of a flat jet, flowing through the narrow nozzle. Liquid lithium in this case is pumped through the heat exchanger. The thickness of such a target is not very crucial and can be 1–2 mm. Such a target device seems more perspective because with temperature of liquid lithium ~ 200°C we will not have practically any problems of evaporation ($P_{sat} = 10^{-8}$ when $T = 230$°C) and limits of power removal are defined only by the power of pumping system and heat exchanger.

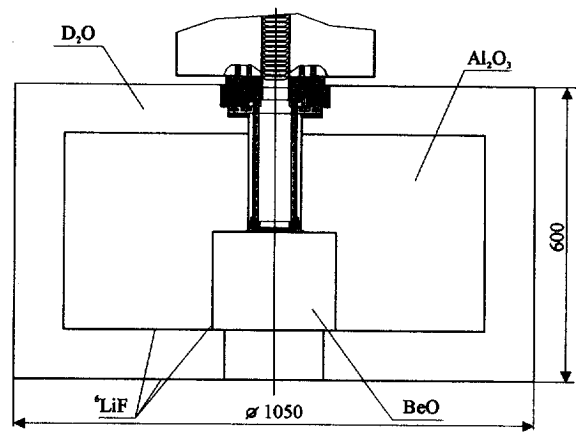

Fig. 17. Target with moderator and reflector.

It should be noted that technical problems of the pumping system and the powerful heat exchanger design in this case are practically similar to ones in target device cooling by intermediate liquid metal heat carriers. There is a big experience at BINP in creation of liquid-lithium pumping systems [40] and jet targets from gallium–indium alloys and liquid lead developed for applications in high-energy physics for secondary particles beam generation [41,42].

7. Conclusion

A project of the proton accelerator complex for fast neutron therapy and for neutron-capture therapy is proposed and discussed in detail.

This project is based on the experience accumulated at IPPE and BINP in following directions:

1. The experimental and theoretical investigations of the spatial-energy distribution of neutrons produced in the $^7Li(p,n)^7Be$ reaction. The proposal to use near-threshold $^7Li(p,n)^7Be$ reaction as an intense and directed neutron source for BNCT.
2. Great experience accumulated in neutronic calculations of the absorbed dose distributions at FNT and also the promising results of collaboration with MRRC RAMS in the use neutron beams for curing malignant tumors.

3. The project of an electrostatic accelerator tandem without accelerator columns – integral part of generally accepted accelerator scheme, is developed. Specifics of geometry of accelerating electrodes and tandem optics allows to reach maximum reliability in conditions of acceleration of high-current proton beams in continuous mode and allows to ensure optimum conditions of pumping out the charge-exchange target region and to use the reliable gaseous target of continuous operation. Main constructive and technical decisions of tandem construction were tested on a 1 MeV prototype which operates now in the pulsed mode of the H^- ion source and is used as an injector in a synchrotron.
4. It is proposed to use the sectional rectifier (a part of the industrial ELV-type accelerator developed at BINP and widely used for technological aims in Russia and abroad) as a powerful high-voltage source. There is experience of rectifier voltage stabilization with accuracy of 0.1%.
5. Wide experience has been accumulated at BINP in design of negative ion sources of different types and a well-known school of specialists in this field has been formed. It allows to create H^- continuous ion source with current 40 mA in short time.
6. Creation of lithium neutron-producing targets with high (up to several kW cm^{-2}) power density is based on wide experience of BINP in producing cylindrical lenses with solid or liquid lithium and liquid-metal targets applied in high-energy physics for secondary particles beam generation.

There is a pool of experience in IPPE in dealing with proton beams of considered range of parameters, and there is a 2 MeV electrostatic accelerator with 2 mA current in Obninsk. Experimental works on optimization of lithium targets parameters and neutron beam forming both in "open" geometry and using moderators and reflectors can be carried out with this accelerator.

All the aforesaid assures that the proposed accelerator complex can be created and transferred for use in clinics within 1.5–2 y.

References

[1] G.L. Locher, Am. J. Roentgenol. 36 (1936) 1.
[2] R.V. Dorn, Int. J. Rad. Oncol. Biol. Phys. 28 (1994) 1189.
[3] R.F. Barth, A.H. Soloway, R.G. Fairchild, R.M. Brugger, Cancer 70 (1992) 2995.
[4] G.A. Miller, N.E. Hertel, B.W. Wehring, J.L. Horton, Nucl. Technol. 103 (1993) 320.
[5] Yu.S. Mardinsky, A.S. Sysoev, V.G. Andreeb, I.A. Gulidov, Strahlentherapie onkologie 3 (1991).
[6] H.B. Liu, R.M. Brugger, D.D. Greenberg, D.C. Rorer, J.P. Hu, H.M. Hauptman, Int. J. Rad. Oncol. Biol. Phys. 28 (1994) 1149.
[7] W.A. Neuman, J.L. Jones, Nucl. Technol. 92 (1990) 77.
[8] R.M. Brugger, J.A. Shih, H.B. Liu, Nucl. Technol. 98 (1992) 322.
[9] A.V. Bondarenko, V.M. Litiaev, Yu.V. Matveev et al., Institute of Physics and Power Engineering, Obninsk, Russia, Preprint FEI-2449, 1995.
[10] J.C. Yanch, X.L. Zhou, R.E. Shefer, R.E. Klinkowstein, Med. Phys. 19 (1992) 709.
[11] C.K. Wang, T.E. Blue, R.A. Gahbauer, Nucl. Technol. 84 (1989) 93.
[12] T.B. Marion, J.L. Fowler (Eds.), Fast Neutron Physics, Interscience, New York, 1960.
[13] V.N. Kononov et al., Proc. 2nd All-Union Symp. on Use of Charged Particle Accelerators in National Economy, Leningrad, USSR, 1–3 October 1975; 2 (1976) 60 (in Russian).
[14] V.N. Kononov, E.D. Poletaev, B.D. Yurlov, Sov. At. Energy 43 (1977) 947.
[15] V.N. Kononov et al., Proc. 1st Workshop on Accelerator-Based Neutron Sources for BNCT, vol. 2, 11-14 September 1994, Jackson, USA, CONF-94096, p. 447.
[16] V.N. Kononov, V.I. Regushevsky, N.A. Soloviov, in: B. Larsson, J. Crawford, R. Weinreich (Eds.), Advances in Neutron Capture Therapy, vol. 1, Medicine and Physics, Elsevier Science, Amsterdam, 1997, p. 528-531.
[17] H. Liskien, A. Paulsen, Nuclear Data Tables 15 (1975) 1.
[18] V.N. Kononov, A.A. Metliov, Institute of Physics and Power Engineering, Obninsk, Russia, Preprint FEI-338, 1972.
[19] E. Segre (Ed.), Experimental Nuclear Physics, vol. 1, New York, London, 1953.
[20] L.N. Rozanov, Vacuum Technology, Vysshaja shcola, Moscow, 1990 (in Russian).
[21] A.A. Glazcov, G.L. Saksagansky, Vacuum of the Electro-Physical Enviroments and complexs, Energoatomizdat, Moscow, 1985 (in Russian).
[22] Yu.I. Golubenko, M.E. Veis, N.K. Kuksanov et al., Budker Institute of Nuclear Physics, Novosibirsk, Russia, Preprint BINP 97-7, 1997.
[23] G. Kuznetsov, Nucl. Instr. Meth. Res. A340 (1994) 204.
[24] Yu.I. Bel'chenko, G.I. Dimov, V.G. Dudnikov, Proc. Symp. on Production and Neutralization of Neg. Hydrogen Ions and Beams, Brookhaven, 1977, BNL 50727, p. 79.

[25] J. Los, E.A. Overbosch, J. van Wunnik, Proc. 2nd Int. Symp. on Production and Neutralization of Neg. Hydrogen Ions and Beams, Brookhaven, 1980, BNL 51304, p. 23.
[26] K.W. Ehlers, K.N. Leung, AIP Conf. Proc. 111 (1984) 258.
[27] G.S. Tompa, W.E. Carr, M. Seide, Appl. Phys. Lett. 48 (1986) 1048.
[28] M. Seidl, W.E. Carr, J.L. Lopes et al., AIP Conf. Proc. 158 (1987) 432.
[29] M. Seidl, H.L. Cui, J.D. Isenberg et al., AIP Conf. Proc. 287 (1992) 25.
[30] J.D. Isenberg, H.J. Kwon, M. Seidl, AIP Conf. Proc. 287 (1992) 38.
[31] K.W. Ehlers, K.N. Leung, Proc. 2nd Int. Symp. on Production and Neutralization of Neg. Hydrogen Ions and Beams, Brookhaven, 1980, BNL 51304, p. 198.
[32] K.N. Leung, K.W. Ehlers, Ibid, p. 65.
[33] B. Piosczyk, G. Dammertz, Rev. Sci. Instr. 57 (1986) 840.
[34] G.I. Dimov, AIP Conf. Proc. 210 (1990) 651.
[35] C.W. Schmidt, C.D. Curtis, Proc. Symp. on Production and Neutralization of Neg. Hydrogen Ions and Beams, Brookhaven, 1977, BNL 50727, p. 123.
[36] G.I. Dimov, Rev. Sci. Instr. 67 (1996) 3393.
[37] R.L. York, R.R. Stevens, AIP Conf. Proc. 111 (1983) 410.
[38] S. Fucumoro, Z. Igarachi, K. Ikegami et al., Proc. 13th Int. Conf. on High Energy Accelerators, Novosibirsk, Russia, 1986; 1 (1987) 293.
[39] S.S. Kutateladze, Heat Transfer and Hydrodynamics Resistance, Energoatomizdat, Moscow, 1990.
[40] B.F. Bayanov, G.I. Silvestrov et al., Proc. 1st European Particle Accelerator Conf., Rome, Italy, 1-11 June, 1988, vol. 1, p. 265.
[41] G.I. Silvestrov, Proc. 13th Int. Conf. High Energy Accelerator, vol. 2, Novosibirsk, Russia, 7-11 August, 1987, pp. 258.
[42] G.I. Silvestrov, Proc. Workshop on New Kinds of Positron Source for Linear Colliders, Stanford University, Stanford, California, 4–7 March, 1997, SLAC 94309, p. 346.